ES97N Project Dissertation

A Smart Regulator to Promote Safety and Wellbeing in Diving

By Matteo Rochon Cocchiara

Warwick ID: 5589746

Supervisor: Professor Julian Gardner FREng FRS

Co-supervisor: Dr Siavash Esfahani

Word count (excluding front matter, references, and appendices): 8935

Total word count: 12994

Originality Statement

"*I hereby certify that this dissertation has been written by me, and that it is the record of work carried out by me, or principally by myself in collaboration with others as acknowledged, and that it has not been submitted in any previous application for a higher degree*."

Signed: Matteo Cocchiara Date: 03 Sept. 2024.

Acknowledgements

I would first like to thank my two supervisors, Professor Julian Gardner and Dr Siavash Esfahani, for generously providing guidance and support both in this project and my broader academic career. I am tremendously fortunate to have two supervisors who are so personally invested in my success, and I am very grateful to them both.

I would also like to thank the kind and supportive team of Warwick's Microsensors and Bioelectronics Laboratory with whom I had the pleasure of working this year. I am especially thankful to Frank Courtney for selflessly lending his time and expertise to helping me redesign the case for the sensor array. Thanks also to Marina Cole, Karthick Kannan Padmanathan, Usman Yaqoob, Barbara Urasinska-Wojcik, and Addison Tian for their advice and good humour throughout the year. I am also indebted to the Engineering Build Space Team who were unwaveringly kind and patient on the many occasions this year when I sought their advice.

Finally, I would like to thank my family. You are my North Star, the guiding light that motivates me to push myself every single day. Special thanks to Anna, my little sister; I'm so proud of you.

Abstract

Despite the popularity of SCUBA (self-contained underwater breathing apparatus) diving, it remains a high-risk pastime for those who undertake it. Two of the most common challenges associated with SCUBA diving are unexpected depletion of the compressed air supply, and carbon dioxide toxicity induced by an abnormal breathing pattern. This study proposes a framework for designing a breath analysis tool to guard against these two issues and promote diver wellbeing through tracking caloric expenditure. This device (termed "smart regulator") will replace the function of a conventional second-stage SCUBA regulator and will analyse data from exhaled breath to achieve the three intended aims. This report starts by summarising the problems facing SCUBA divers, and the key features of a viable solution. A literature review in Section 2 then uses available studies on indirect calorimetry and breath monitoring to provide some preliminary guidelines for subsequent design stages. Section 3 of the report then proposes and describes a potential solution which is later validated through simulations and calculations. A detailed explanation of how the sensor outputs can be applied to the realisation of the three device aims is provided in Section 4. The results and limitations of the study are discussed in Section 5, followed by conclusory remarks and suggestions for further work in Section 6.

Contents

List of Tables

List of Figures

Section 1: Introduction and Problem Definition

1.1 - Introduction

SCUBA (an acronym of "Self-Contained Underwater Breathing Apparatus) diving is a common pastime amongst adventure seekers, undertaken for both experiential enjoyment and perceived health benefits [1], [2]. Despite this popularity, SCUBA diving remains a comparatively dangerous hobby with approximately two deaths per 100 000 dives [3], and many more injuries and near misses [4]. As a result, several studies have attempted to identify means of increasing the safety of SCUBA diving, either through the development of new technology [5], or through educational and legislative efforts [6]. This study describes the creation of a novel breath analysis device (a smart regulator) which aims to enhance diver safety and wellbeing in three ways: monitoring of expired gas volume; identification of abnormal breathing patterns; and calculation of energy expenditure.

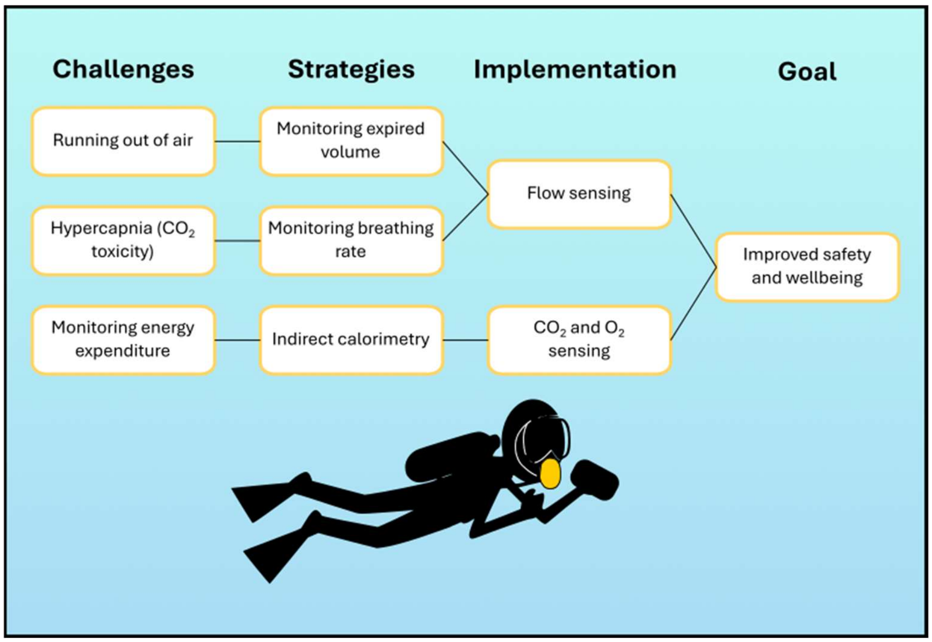

Figure 1: An illustration showing how realisation of the different sub-goals of this project contribute to the broader aim of improving safety and wellbeing.

The use of compressed gases to enable underwater breathing creates several vulnerabilities that can endanger SCUBA divers. One of the most common is unexpected depletion of the compressed gas supply, an event that often leads to injury and death [7], [8]. Another issue in SCUBA diving is carbon dioxide (CO_2) toxicity, also known as hypercapnia or hypercarbia: this occurs when CO_2 levels in the blood exceed normal physiological limits, causing mental confusion, loss of consciousness, and death [9]. Abnormal respiratory patterns are believed to spur hypercapnia by increasing carbon dioxide retention, eventually causing the pathological levels associated with symptom onset [9], [10]. This information suggests that measuring the volume flow rate (VFR) at the outflow of the SCUBA apparatus could be tremendously helpful in safeguarding against these dangers, since it could allow both respiratory rhythm and expired volume to be tracked; these are two of the three core functions of the proposed device.

However, the opportunities for the proposed technology extend beyond simply measuring gas flow: expired breath analysis is a widely used technique in healthcare, and is attractive for its versatility, high information yield, and relative non-invasiveness [11], [12]. One common application of breath analysis in medicine is indirect calorimetry, a term which refers to the use of respiratory gases to estimate bodily energy expenditure [13]. Thus, inclusion of carbon dioxide (CO_2) and oxygen (O_2) sensors could allow estimation of energy expenditure, providing an added boost to the user's wellbeing; this is the third and final function of the proposed device.

The rest of Section 1 focuses on providing a technical description of the problem to clarify the aims of the project from an engineering perspective. Afterwards, the remainder of this report is split into five sections. First, a literature review in Section 2 distils relevant findings from a broad range of literature sources to derive relevant design recommendations. Section 3 lists the user and technical requirements of the device, then recommends and validates a potential solution through calculations and finite element modelling. In Section 4, a framework is presented for converting the sensor outputs to achievement of the intended device aims. Section 5 then examines the main findings and limitations of the study, alongside a brief discussion of relevant commercial considerations. Finally, Section 6 provides some conclusory remarks, and proposes opportunities for further study.

1.2 – Key elements of a viable solution

Table 1: A tabulation of the key requirements of the proposed device.

Factor	Minimum requirement	Rationale
O_2 sensor range	0 – 21%	Exhaled air typically contains 16% O_2 (compared to the 21% in atmospheric air [14]). However, it is reasonable to use the higher of these two values as the upper bound of the sensor requirement.
CO_2 sensor range	0 – 8%	Exhaled air is usually 4-5% CO_2, [15] but it is reasonable to add a slight buffer to ensure that the sensor is not operating at the edge of its effective range.
Volatile organic compound (VOC) sensor range	No minimum (see rationale)	As will be outlined in Section 3.1.3, the VOC sensor has been included in the design to assess the viability of substituting the electrochemical oxygen sensor for the VOC sensor.
Air speed sensor range	0 - 13ms^{-1}	There is flexibility in the air speed sensor range since the width of the channel housing the sensor can be adjusted to optimally exploit its range. The upper limit was chosen based on a 2017 study by Mhetre and Abhyankar [16] which found that air could reach a velocity of up to 10ms^{-1} during forceful exhalation..
Pressure sensor range	1 – 4 bar	A pressure of 4 bar corresponds to a submerged depth of around 30m which is the upper limit of what would be typical for the intended market (recreational scuba divers).
Temperature sensor range	-5 - 35°C	Due to the challenges of diving in extreme temperatures, it is unlikely that recreational divers would be subject to temperatures outside this range.
Humidity sensor range	0 – 100% relative humidity	The relative humidity of exhaled breath can range from 42 to 91% [17], so the limits of the humidity sensor should reflect this variability.
Battery life	3 hours	Recreational dives typically last about one hour [18], but a buffer should be incorporated to minimise the risk of unexpected power loss.
Case pressure tolerance	0 – 7 bar	Due to the unpredictability of operating in extreme environments, the pressure tolerance of the case should markedly exceed the expected loads.

Section 2: Literature Review

The aim of this review is to analyse existing research to synthesise design recommendations for the present study. Two key domains were identified as having high relevance to the proposed device: indirect calorimetry and breath monitoring. Accordingly, the section is split into two parts, with each focused on one of these two thematic areas. The subsections will include a summary of relevant findings from the literature, followed by a discursive paragraph that aims to extract design guidelines.

2.1 – Indirect Calorimetry

A review of the literature on the subject of indirect calorimetry highlights two classes of methods that would be relevant to this study [19]: mixing chamber and breath-by-breath approaches. As noted by Macfarlane [20], mixing chamber indirect calorimetry was developed first because carbon dioxide sensors at the time were too slow to reliably enable analysis of individual breaths. By pooling multiple breaths in a mixing chamber, the need for fast-acting sensors was removed, and devices gained superior accuracy and robustness to outliers. These incentives continue to drive the adoption of mixing-chamber approaches by some groups, with a recent example being the Carbon-dioxide Oxygen Breath Respiration Analyzer (COBRA) from Candell *et al.* [21].

As carbon dioxide sensors improved, some devices started omitting the mixing chamber and instead relied on fast-acting sensors to pick up concentration changes in real time: these were known as breath-by-breath (or BxB) systems. Although earlier studies showed that breath-by-breath systems did not perform as well as laboratory-accredited metabolic carts [22], [23], more recent work generally suggests that modern devices can produce results consistent with those of the gold standard [24], [25], [26]. However, it should be noted that several studies show BxB techniques exhibit significant errors at higher exercise intensities [25], [27], [28], and are less accurate than mixing chamber systems [28], [29]. Recent efforts in BxB system design have focused on the production of more consumer-friendly devices rather than expensive research tools. For example, a 2016 paper by Vincent *et al.* describes the development of a smartphone-compatible BxB system consisting almost entirely of off-the-shelf parts [30].

Based on the available literature, it was decided that a mixing chamber approach to indirect calorimetry would be the best fit for this project. Accuracy is the main driver of the decision and is an especially relevant factor given that the relative concentrations of key gases (i.e. carbon dioxide and oxygen) could be much lower than those at surface level if specialised gas mixes are used. As an added benefit, the use of a mixing chamber system obviates the need for high-speed sensors, likely enabling the product to be offered at a markedly lower cost.

2.2: Respiratory rate monitoring

According to Bube *et al*. [5], two studies have attempted to track breathing rate in SCUBA diving: a 2017 study by Altepe *et al* and a 2019 study by Eun *et al.*. The former group monitored changes of intermediate pressure in the buoyancy compensator device of the diver. This allowed them to identify their participants' inhalations and, by extension, dangerous breathing rhythms such as hyperventilation and "skip breathing" (the insertion of an artificial pause between inhalation and exhalation). This technique was successful in identifying inhalation (with a global sensitivity of 97%), but no protocol was incorporated to test the device's capacity to identify abnormal breathing patterns. The 2019 study by Eun *et al.* [31] used a textile-embedded sensor placed over the sternum to monitor breathing rate. Unfortunately, the lack of similarity to the present work, coupled with the limited detail provided about the design, prevents this work from providing useful frameworks for design of the smart regulator.

Outside SCUBA diving, respiratory rate (RR) monitoring is widely acknowledged as a valuable physiological variable in healthcare. Indeed, reviews in 2017 and 2020 by Nicolò *et al.,* suggest that RR can be used to track both chronic and acute conditions [32], and also has applications in non-medical fields such as sports science [33]. This wealth of uses has incentivised researchers to design a range of both contact and non-contact methods of respiratory monitoring [34], [35], including the use of flow sensors to track air influx and efflux. An example of this approach is a 2019 paper by Jiang *et al.* [36] which used a hot wire flow sensor to detect changes in respiratory airflow associated with obstructive sleep apnoea syndrome.

The limited number of papers that focus on breath monitoring in the context of SCUBA diving means that there is no strong basis on which to favour any single design approach. This is supported by the wide range of potential strategies that have been adopted outside of SCUBA: indeed, a 2019 paper by Massaroni *et al.* mentions more than twenty contact-based methods of measuring breathing frequency [35]. Thus, given that flow sensors have been previously applied in breath monitoring [36], their inclusion in the proposed device is valid.

Section 3: Design

3.1 – Identification of requirements

3.1.1: User requirements and relevant design requirements

Table 2: A tabulation of the user requirements of the proposed device alongside their corresponding design requirements. User requirements were identified on the basis of their direct relevance to the three stated key aims.

#	User Requirement	Design Requirements
U.1	The device can estimate the quantity of gas expired	• Flow speed sensor • Temperature sensor • Pressure sensor • Channel of known cross-sectional area • Microcontroller • Gas outflow algorithm
U.2	The device can identify skip breathing and hyperventilation	• Flow speed sensor • Microcontroller • Abnormal breathing pattern algorithm
U.3	The device can estimate the caloric expenditure of the user	• Carbon dioxide sensor • Volatile organic compound (VOC) sensor • Oxygen sensor • Mixing chamber of a known volume • Microcontroller • Caloric expenditure calculation algorithm

3.1.2: Technical requirements

Table 3: A tabulation of the technical requirements underpinning the design of the proposed device. Each technical requirement is listed alongside its means of verification (where applicable).

Category	#	Requirement	Verification
General	A.1	The projected bulk cost of the final unit should be less than 160 GBP	Cost projection (c.f. Section 7.1)
Input	B.1	The device should incorporate a means of extracting a 50ml sample from each breath	Factored into sampling system design (c.f. Section 3.2.4)
Output	C.1	Digital output of a three-hour dive should fit on a 32GB Secure Digital Memory card (SD card)	Numerical calculation post design (c.f. Section 3.3.5)
	C.2	All sensor outputs should be compatible with an Adafruit ESP32-S3	Factored into sensor selection (c.f. Section 3.2.2)
	C.3	All gas concentration sensors should have a T_{90} response time that is less than or equal to 7.5 seconds	Factored into sensor selection (c.f. Section 3.2.2)
	C.4	The flow sensor should be capable of tracking flow speed in real time	Factored into sensor selection (c.f. Section 3.2.2)
Conditions	D.1	The sensors should maintain 90% accuracy at temperatures ranging from 0°C to 40°C	Testing required by future studies (c.f. Section 6.2)
	D.2	The sensors should maintain 90% accuracy at pressures ranging from 1 to 4 bar	Testing required by future studies (c.f. Section 6.2)
	D.3	The final design should be waterproof up to a depth of four atmospheres	Testing required by future studies (c.f. Section 6.2)
	D.4	The case material should be able to withstand the forces associated with underwater immersion at a depth of 60m with a minimum safety factor greater than three.	Finite element simulations (c.f. Section 3.3.2)
	D.5	The sensors should maintain 90% accuracy at pressures ranging from 1 to 4 bar	Testing required by future studies (c.f. Section 6.2)

Material	E.1	The case material should not display significant physical or mechanical degradation in seawater over a span of two years.	Factored into material selection (c.f. Section 3.2.3)
	E.2	The middle of the case should be able to recover to from a 30°C thermal shock in less than one minute.	Finite element simulations (c.f. Section 3.3.1)
Usability	F.1	The device should be comfortable for a diver to wear for at least three hours	Testing required by future studies (c.f. Section 6.2)
	F.2	The device should either have neutral or negative buoyancy	Buoyancy assessment (c.f. Section 3.3.3)
	F.3	The device should have a display to communicate relevant information	Factored into PCB design (c.f. Section 3.2.5)
	F.4	The device should be able to operate continuously during a three-hour dive without risk of depleting a AAA battery.	Numerical calculation post design (c.f. Section 3.3.4)
Case	G.1	The mixing chamber should be able to accommodate samples of five breaths	Factored into case design (c.f. Section 3.2.1)
	G.2	The case should have space to store a standard PP3 battery	Factored into case design (c.f. Section 3.2.1)
	G.3	The case should incorporate a strap, or other means of attachment to the diver	Factored into case design (c.f. Section 3.2.1)
	G.4	The case should include a means of attaching the PCB to the case body	Factored into case design (c.f. Section 3.2.1)
Performance	H.1	The device should be able to estimate the volume of expired gas with an accuracy of at least 90%	Testing required by future studies (c.f. Section 6.2)
	H.2	The device should be able to identify abnormal breathing patterns (skip breathing and hyperventilation) with sensitivity and accuracy values of at least 90%	Testing required by future studies (c.f. Section 6.2)
	H.3	The device should be able to estimate caloric expenditure using the abbreviated Weir Equation with an accuracy of at least 90%	Testing required by future studies (c.f. Section 6.2)

3.1.3 – Optimisation

If the minimum viable product (MVP) addresses the requirements outlined in Sections 2.1.1 and 2.1.2, the device will be optimised for improved user comfort and lower production cost. The former will be achieved by replacing the strap-based design demanded in Requirement A.2 with one that attaches directly to the existing second-stage regulator. The production cost will be reduced by two methods 1) the replacement of components and materials for cheaper alternatives 2) the removal (if appropriate) of the electrochemical oxygen sensor. This second modification will only be justified if the VOC concentration is sufficiently low that the output of the metal oxide VOC sensor depends solely on the concentration of oxygen, thus allowing the VOC sensor to substitute the oxygen sensor.

This simplification is predicated on the operating mechanism of n-type metal oxide sensors: as Lin *et al.* describe in their 2019 work, adsorbed gaseous oxygen is reduced to a set of lower oxidation states including O_2^-, O^-, and O^{2-} [37]. This removal of electrons from the conduction band results in a temporary loss of conductivity which can be restored if reducing gases (such as VOCs) react with the adsorbed oxygen ions [38]. However, in the absence of such gases, the resistance of the semiconductor will depend exclusively on the concentration of oxygen, allowing the metal oxide sensor to substitute the role of the electrochemical oxygen sensor.

3.2 – Hardware Design

3.2.1: Case design

Although this project eventually seeks to integrate the whole device directly into the body of the regulator, the creation of a secondary apparatus to house the sensor array provides greater design flexibility for the design of a minimum viable product. As a starting point, inspiration was taken from Altepe *et al.* [10], whose 2017 study used a recording system that was wholly separate from standard SCUBA equipment. In their work, a pressure sensor array was housed in a sealed metal case which was worn above the diver's left arm, and this allowed the diver's breathing to be monitored.

Initially, the present study adopted a similar structure to that chosen by Altepe *et al.*, but several changes had to be made to account for the desired functional differences. Additionally greater flexibility was permitted with regards to the material selection, since this study aimed to produce a device which could, at least in theory, be suitable for manufacturing at scale. For this reason, two versions of the case proceeded to the validation stage: one made entirely of plastic, and another which featured a metal exterior shell. Technical Requirements G.1-4 drove the design of the case prototype: Figure 2 shows the ways in which they were implemented in the final design.

Although the main components of the case remained the same, the design underwent several iterations as new constraints were imposed by the choice of hardware, the testing parameters, and the need to maintain an airtight and watertight seal. Overall, the structure of the case produced by the end of this study is a close approximation of the envisioned design. However, the body of the case was made of polylactic acid (PLA), even though this does not match the outcome of the material selection and simulation processes (c.f. Sections 3.2.3 and 3.3.1-2). This was done because it was intended that the case would be tested at room temperature and pressure, making the device performance largely independent of case material. Furthermore, the use of PLA allowed for easier prototyping using a 3D printer, allowing several iterations to be produced over the course of the design process.

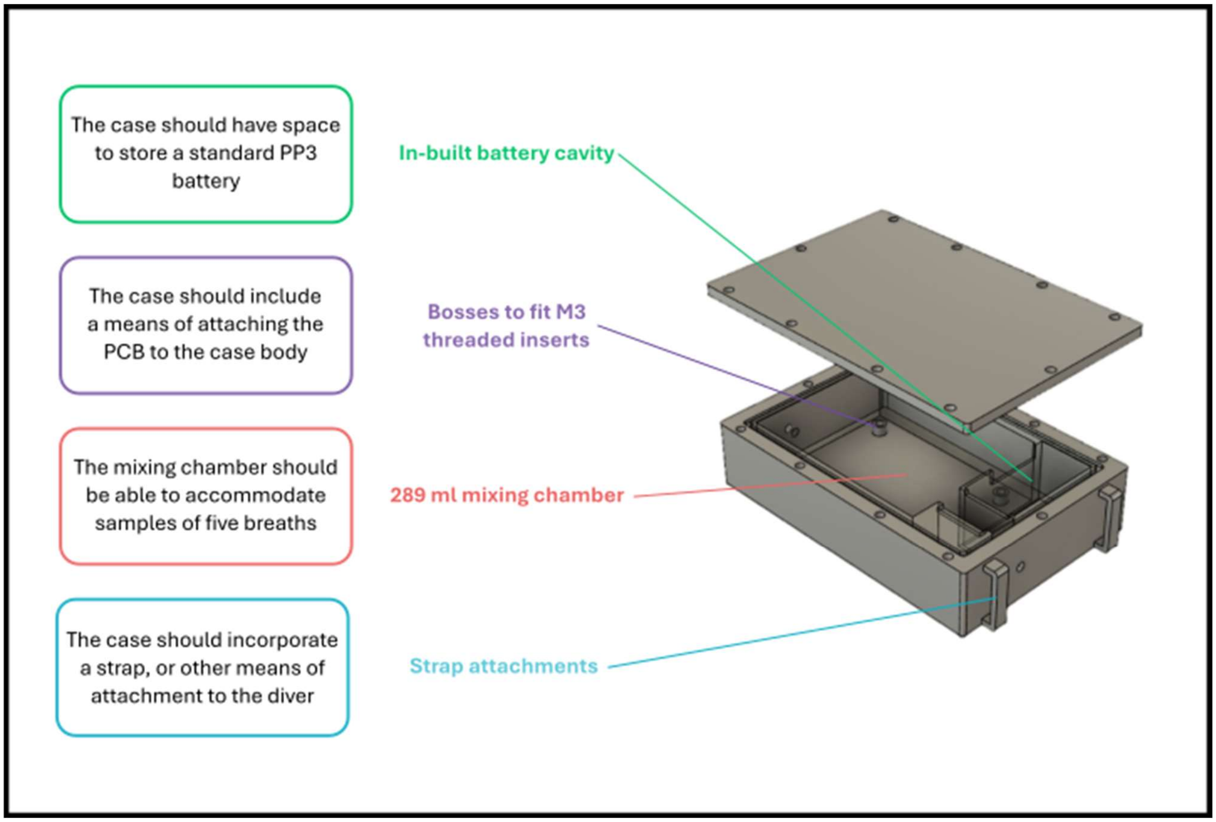

Figure 2: A diagram showing how the four relevant design requirements (G.1-4) were incorporated into the case.

3.2.2: Sensor selection

Based on the user requirements (c.f. Section 3.1.1), it was determined that sensors for the following variables would be needed: oxygen concentration ($[O_2]$), carbon dioxide concentration ($[CO_2]$), VOC concentration ($[VOC]$), temperature (T), pressure (P), and flow speed (v). Since a variety of sensors could fulfil each of these functions, the constraints from Sections 1.2 and 3.1.2 were used to limit the range of potential options. The final selections are displayed in Figure 3, along with their locations and connections; the technical specifications of the sensors are provided in Appendix A.

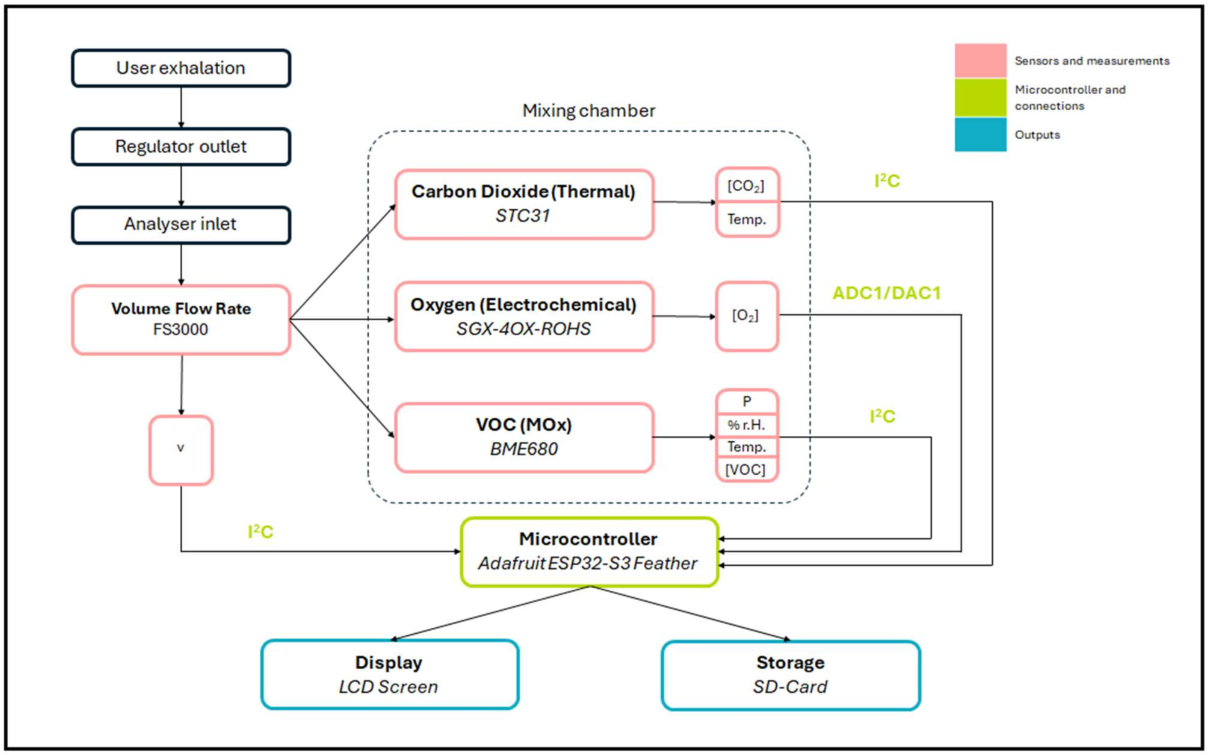

Figure 3: A diagram showing the information flow from the sensors to the microcontroller to the outputs.

3.2.3: Material selection

The primary technical requirement underpinning material selection was E.1, since it was believed that resistance to corrosion would impose the strictest limit on the range of available materials. Hence, a brief literature search was conducted to find three plastics and three metal alloys that have been shown to undergo minimal degradation in seawater. The results of this search are shown in Table 4.

The information in Table 4 suggests that there is relatively little variation in the mechanical and thermal properties of candidate polymers. Polycaprolactone can be immediately ruled out, since it is the lightest, least stiff, and most expensive, thus making it unsuited for an application where low cost and high mechanical stability are of primary importance. The remaining two candidates are similar in almost all respects, but the lower expected cost of polyethylene terephthalate (PET) gives it a small edge in appeal over polylactic acid (despite the slightly lower density of the latter). Based on these factors, PET was identified as the most appropriate material for the present study and was adopted in subsequent thermal and mechanical simulations.

The main advantage of choosing aluminium or titanium alloys over stainless steel is the reduction of weight enabled by their significantly lower densities (2700 and 4429kg/m^3 respectively compared to 8000kg/m^3). However, since the proposed device will be submerged, the weight of the device will be offset by the upwards force generated due to the displaced water, giving more flexibility in material density. The fact the device will mostly operate under high mechanical loads also lends greater importance to the increased Young's Modulus of stainless steel. Furthermore, although the higher thermal conductivity of aluminium may allow the temperature of the unit to equilibrate more rapidly with the surroundings, further testing is required to confirm the impact this will have on device performance. Based on these factors, and accounting for the relative material costs, 316L stainless steel was selected as the material of choice for the MVP and subsequent thermal and mechanical simulation.

Table 4: Findings from the brief review of suitable materials, as assessed by their tolerance to saltwater corrosion.

Material	Density (kg/m^3)	Tensile Modulus (GPa)	Seawater resistance test conditions	Thermal conductivity (W/mK)	Price per kg (USD)
Polycaprolactone (PCL)	1070-1200 [39]	0.20-1.38 [39]	Artificial seawater [40]	0.2 [41]	6-8 [42]
Polylactic acid (PLA)	1210-1290 [39]	2.7-16.0 [39]	Artificial seawater [40]	0.183 [43]	0.84-3.55 [44]
Polyethylene terephthalate (PET)	1300-1400 [39]	2.3-17.9 [39]	Artificial seawater [40]	0.1888-0.3300 [39]	0.55-0.90 [45]
316L Stainless Steel	8000 [46]	193[46]	Artificial seawater with mechanical friction stimulus [47]	16.3 [46]	3.98 [48]
Aluminium AA5083	2700 [49]	72 [50]	Seawater [51]	120 [52]	18.06 [48]
Titanium 6Al-4V	4429 [53]	71 [54]	Artificial seawater with mechanical friction stimulus [47]	6.60 [55]	26.59 [56]

3.2.4: Sampling system design

The requirement for averaging over multiple breaths, combined with the small size of the mixing chamber, makes it challenging to isolate the small volume of breath needed for analysis. A healthy adult will exhale between 400ml and 500ml [57] of breath at atmospheric temperature and pressure: thus, a sampling system is needed that can separate about one tenth of the total breath volume. Although several solutions were considered initially, many of them would have required time-intensive modelling, or assumptions that could not be easily substantiated. By contrast, the final method selected in this study provides an elegant initial solution which can be easily modified and reiterated as the device is developed further.

The sampling system is predicated on the use of two channels (one for testing, one for exhaust gas) which are sized in proportion to their desired outflow volume. Hence, since the testing volume is one tenth of the total gas exhaled, the exhaust outflow should have nine times the surface area of the testing outflow.

The second-stage SCUBA regulator provides a useful way to implement this principle: breath outflow from the regulator is ordinarily controlled by a single umbrella valve which opens only when its membrane pressure is exceeded. By adding a second, smaller outlet and covering it with an umbrella valve of the same membrane pressure, the breath can be split into the desired proportions for testing and exhaust.

Figure 4 shows the proposed sampling system incorporated into a generic second-stage regulator. As can be seen in the bottom right of the figure, the relative sizing of the different outflows should enable the gas to be split into the desired proportions for testing and exhaust. Of course, this will need to be rigorously tested prior to commencing fieldwork: however, given the time constraints of the present project, this report is limited to presenting a theoretical solution.

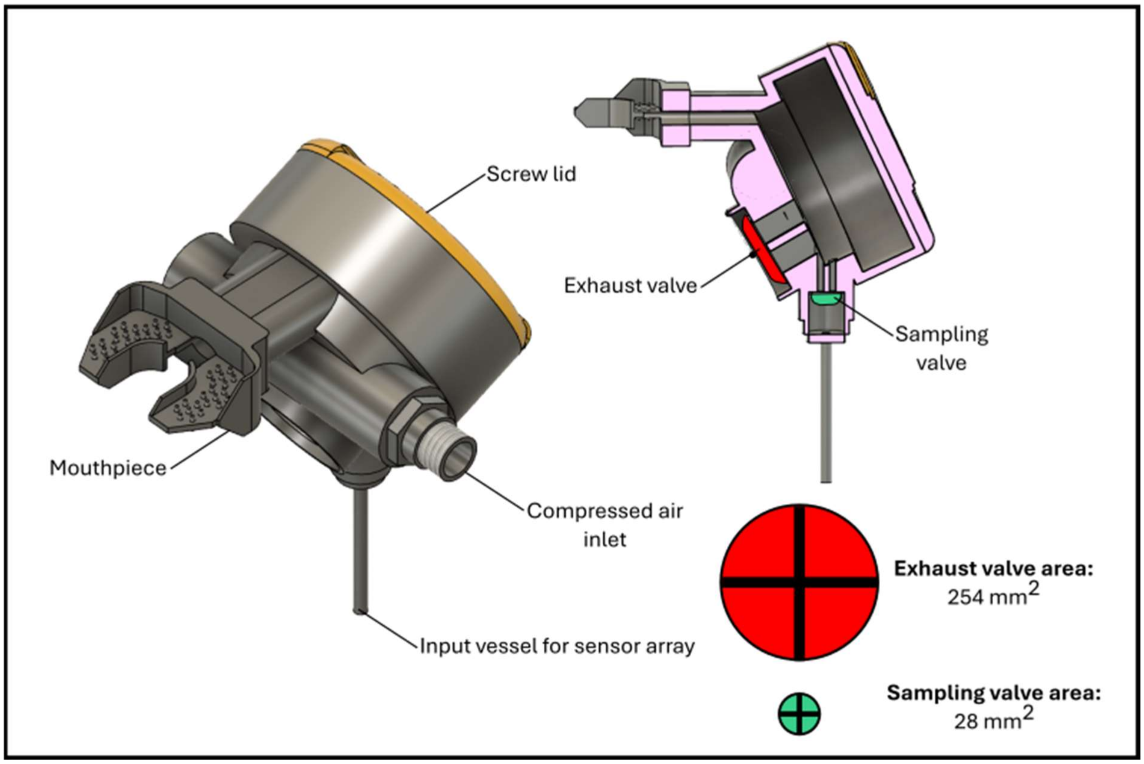

Figure 4: A Fusion 360 model of the sampling system for the smart regulator. The right side of the image shows a cross section of the device with two proportionally sized outlets for sampling and exhaust.

3.2.5: Printed circuit board (PCB) design

Design of the PCB was undertaken by another team member (Dr Siavash Esfahani), so a full description of the process is beyond the scope of this report. Nonetheless, this subsection has been included to highlight the importance of the PCB design in the context of the broader development workflow. After designing the case and choosing appropriate sensors, the author of this report created a layout which showed the area available for a PCB within the mixing chamber of the case, as well as the positions of the attachment points. This was sent to Dr Esfahani, who used the Altium Designer software to place the sensors and microcontroller (Adafruit ESP32-S3 Feather with an integrated LCD screen) at the appropriate positions. The final design was sent for manufacturing, and the components were soldered at the indicated locations by a member of the Warwick University Electronics Support Team.

3.3 – Hardware validation

After these design stages, the hardware underwent a series of validation steps to examine key performance aspects, including assessing the buoyancy of the case, and its capacity to withstand the requisite thermal and mechanical loads. Further calculations were also done to ensure the power supply and data storage capacities of the device would be sufficient for the chosen sensors. The aims of these tests were twofold: firstly, the time-constrained nature of the project means that *in-silico* tests such as these provided valuable design information without the complicated apparatus required by field testing. Secondly, the thermal and mechanical simulations provided data to guide the selection between the all-PET case design and the version with a stainless-steel exterior.

3.3.1: Thermal shock simulation

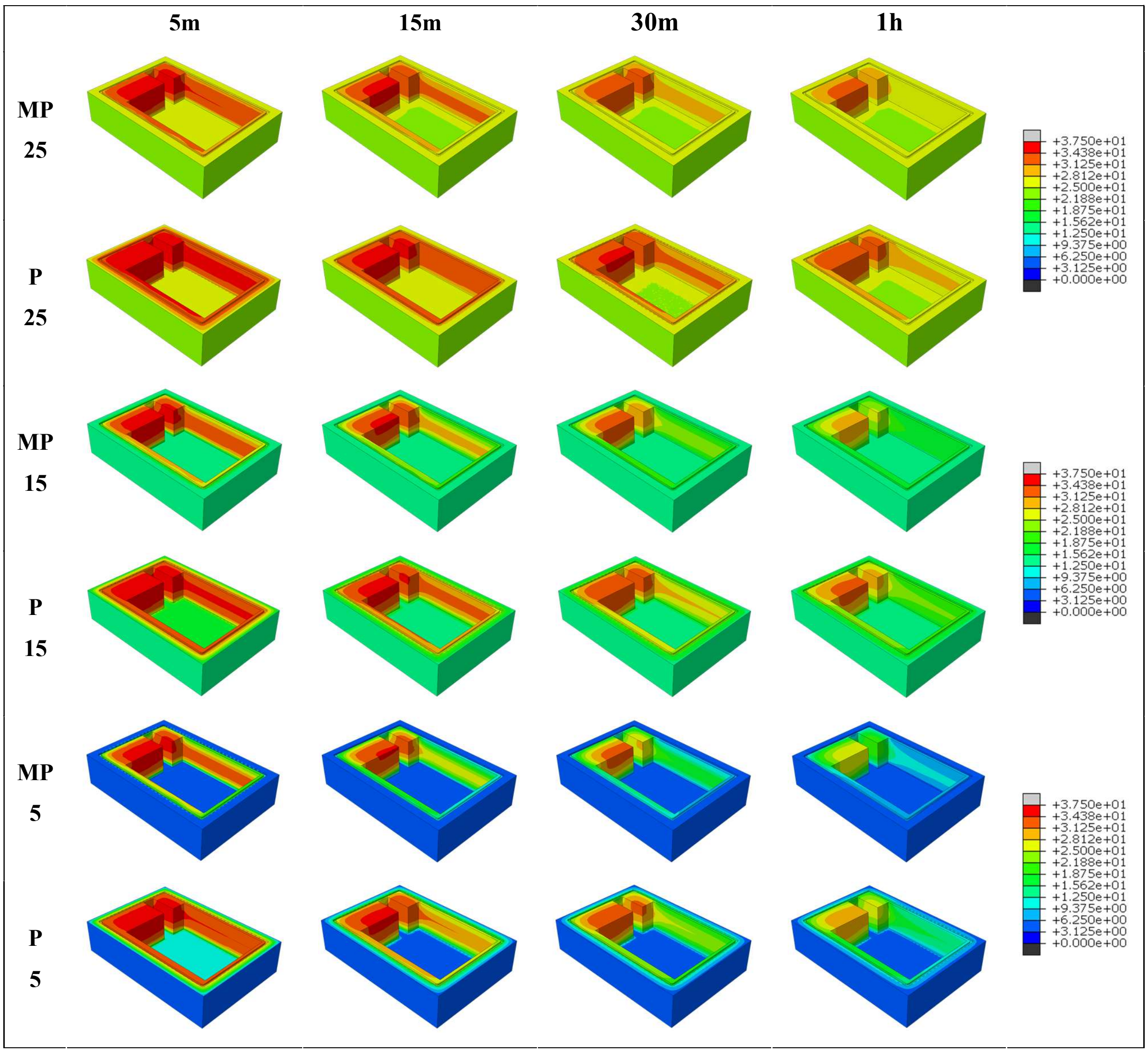

Figure 5: Results of the thermal shock simulations. Each row represents one test, with the columns showing the submersion time Each row has a two-part designation indicating the parameters: the first term indicates the case material (MP = metal and plastic, P = plastic only), and the second term indicates the sink temperature in Celsius. The key on the right shows the temperature in Celsius.

The thermal simulations were conducted to assist with the selection between the steel exterior shell and the PET exterior shell; in both cases, the interior was made of PET. Though it is more expensive, the higher conductivity of stainless steel (c.f. Table 4) will cause the case to thermally equilibrate more rapidly, thus ensuring that the information relayed by the sensors accurately reflects ambient conditions. Hence, the aim of these simulations was to determine whether the faster thermal conduction of the steel exterior justified its increased cost.

Both models were subjected to three sets of thermal stresses designed to simulate underwater submersion of the device. At t = 0s, the apparatus was assumed to be in thermal equilibrium with hot surroundings (35°C): this was specified through the initial conditions. The apparatus was then immediately subjected to convective heat loss via the external surfaces of the case. The temperature of the thermal sink was varied from 25°C (simulating a relatively small temperature jump of -10°C) to 5°C (simulating an atypically large temperature jump of -25°C). Appendix B lists all the simulation parameters used for the Abaqus transient thermal analysis.

Figure 5 shows a summary of the results from the thermal simulations. A superficial inspection of the images would suggest that the steel exterior offers only slight improvements in conductivity over the plastic case, since the temperature difference rarely exceeds a single colour band (~3.1 degrees Celsius). However, by plotting how the temperature of a single node in the middle of the case varies over time, the value of the steel case becomes apparent. This is shown in Figure 6, which demonstrates the dramatically slower thermal equilibration of the plastic case. Indeed, the metal case is able to adjust to within one degree Celsius of the sink temperature in just twenty seconds for even the largest thermal shocks. This contrasts markedly with long cooling time of the all-plastic case which can take several minutes for large changes in temperature.

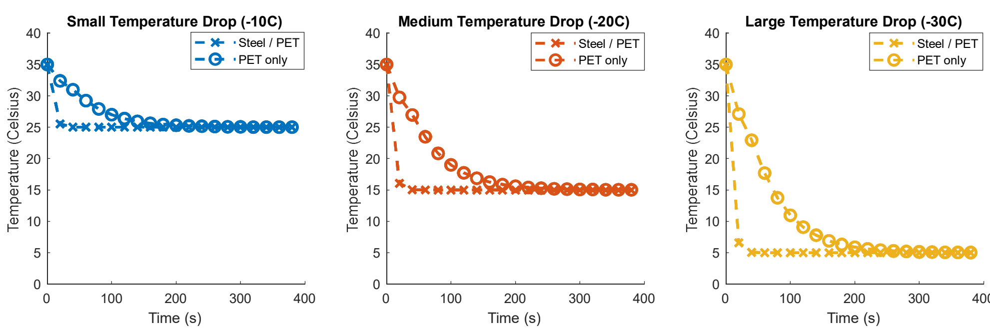

Figure 6: A set of plots showing the temperature at a node in the middle of the case. Note that the steel / PET design adjusts almost instantly to the thermal shock, whereas the addition of PET can add almost five minutes to the equilibration time.

Thus, based on these simulations, it is reasonable to view the steel exterior as a more favourable option than the all-PET design. Subsequent validation stages will examine other aspects of the case performance, including its ability to withstand the requisite mechanical stresses, and maintain buoyancy.

3.3.2: Mechanical simulation

The mechanical performance of both cases (PET-steel and fully PET) was simulated using a static stress test in Autodesk Fusion 360. As with the thermal simulations, the model was simplified by removing any fillets, drill holes, extrusions, or cavities other than the main mixing chamber: this was done to ease modelling and improve computational efficiency.

Two mechanical load cases were simulated for each build (four in total), representing immersion in water at 30m and 60m depth. The top side of the unit was assigned a fixed structural constraint since that is the point where the strap attaches to the case. The hydrostatic pressure was calculated using Equation 1, and this was then multiplied by the area of each load-bearing surface to obtain the force. Yield strength, rather than ultimate tensile strength, was used as the benchmark for the safety factor since plastic deformation would be a severe detriment to the operational lifetime of the device. The full details of the simulation parameters, including the number of nodes and shape function order, are included in Appendix C.

$$p = \rho * g * h \qquad [1]$$

As can be seen in Figure 7, the addition of the steel exterior greatly improves the capacity of the case to withstand the required mechanical loads. Indeed, the minimum safety factors calculated from the metal designs exceed those of the plastic counterparts in all instances. This suggests that the steel case, though slightly more expensive, is likely worthwhile due to its ability to provide a barrier against the variable loads that are prevalent in extreme environments. This impression is further reinforced by the results of the simulations with the all-PET case: a minimum safety factor of 1.56 in the 60m submersion study indicates that the device only marginally withstood the applied load.

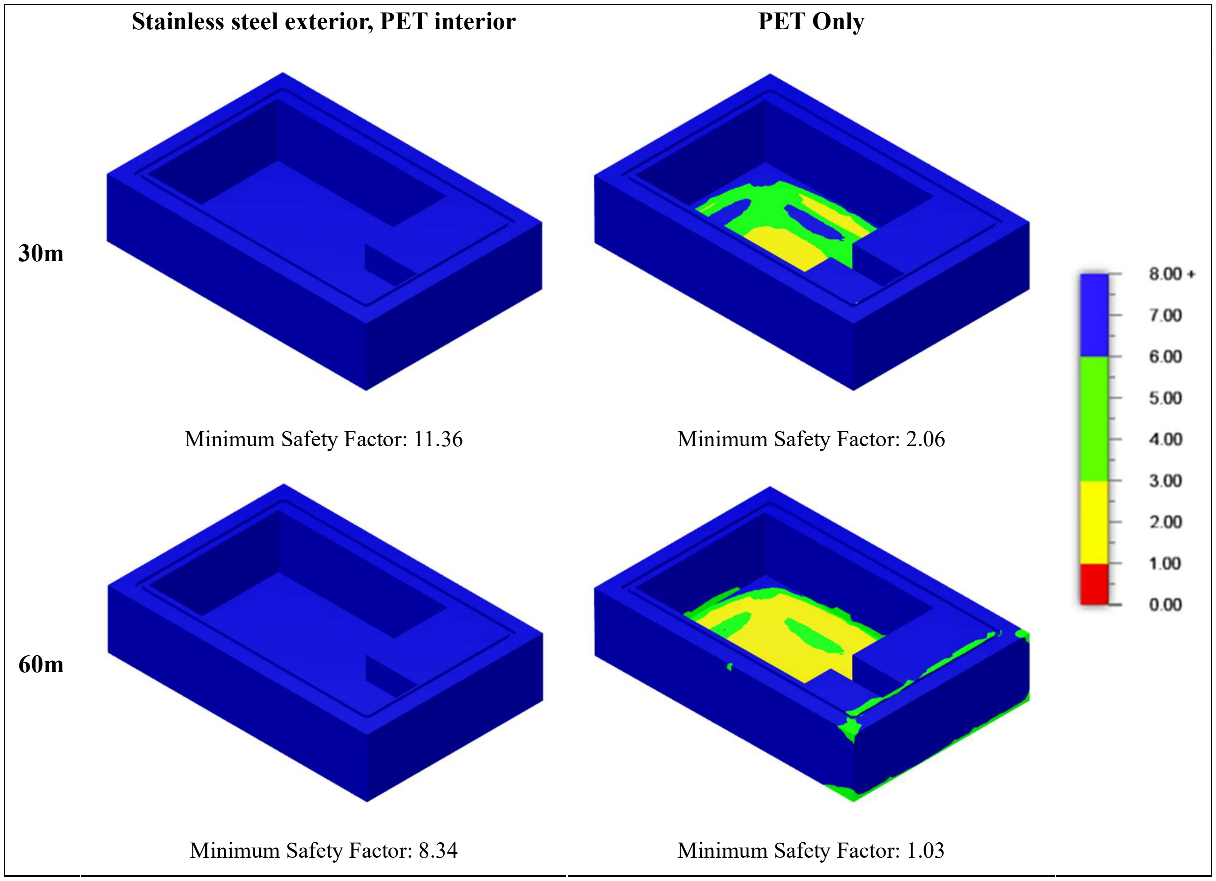

Figure 7: Results of the mechanical simulations on Fusion 360. The row indicates the depth being simulated in metres, whereas the column corresponds to the model (left is stainless steel and plastic, right is plastic only). Note that the PET-only design has a much lower minimum safety factor, as well as a large spread of structurally weak areas along the base.

3.3.3: Buoyancy assessment

As noted in Requirement F.2, the device should either be neutrally or negatively buoyant overall. This is because positive buoyancy would introduce issues for both usability and safety: since buoyant forces have to be carefully counteracted through the use of lead weight belts, the introduction of additional upward forces on the diver is incompatible with the needs of the target market.

The buoyancy of the device was assessed by analysing the weight of the case against the upthrust generated upon immersion into seawater. To add a margin of safety, the weights of individual hardware components (sensors, battery, etc.) were ignored, and the maximum density of seawater (1055 kg/m^3 [58]) was used to calculate upthrust.

The volumes of the case components (stainless steel lid, stainless steel shell, and PET interior) could be found by querying the properties of the relevant bodies in the Fusion 360 model. The (empty) internal volume of the case was found by producing a separate body (c.f. Figure 8) which filled the relevant cavities, and then repeating the process of querying the body properties.

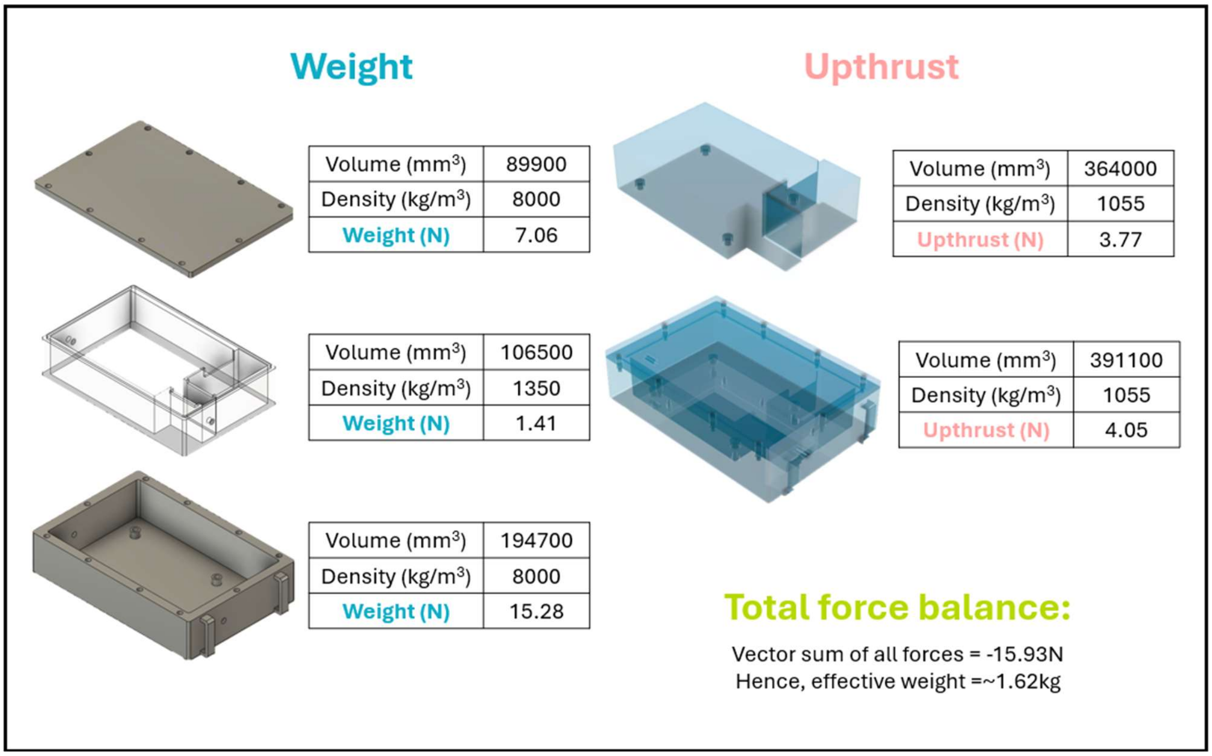

Figure 8: The left-hand column of the figure shows the volumes, densities, and weights of the different case components to calculate the total downwards force generated by the apparatus. The right-hand column calculates the upthrust generated by the weight of the displaced fluid.

As shown in Figure 8, the device is negatively buoyant with an effective weight of about 1.62kg. This negative buoyancy is appropriate for SCUBA diving but may not be compatible with wear using a neck strap as envisioned (particularly if the load is increased by drag on the device while swimming). This is something that should be considered as the device is reiterated and tested. If the load is found to be uncomfortable, different attachment solutions can be proposed, such as fastening the device via a strap to the trunk or waist. Alternatively, selecting one of the lighter metals considered earlier could provide an appropriate solution: replacement of the steel with aluminium would impose an effective negative load of just 2.54N (equivalent to about 250 grams).

3.3.4: Power consumption estimation

The total power requirements of the four sensors add to give 70.5mW (c.f. Appendix A). A typical recreational dive lasts one hour [18], but a longer one may last as long as two hours. Based on this information, and the warmup time of the sensors, it would be reasonable to require three hours of power at a time. Multiplying the per-second power demand (70.5mW) by the number of seconds in three hours, one obtains an energy requirement of 761 Joules, equivalent to 0.21 Watt hours (Wh).

The device will also use an Adafruit ESP32-S3 TFT Feather microcontroller to coordinate the action of the sensors. The Feather requires about 0.132 W during normal operation, equating to an energy consumption of

1425.6 Joules (0.40 Wh) over a three-hour dive. Adding this to the energy demand for the sensors, one obtains a total energy use of 0.61 Wh: this is approximately one third of the energy stored in a typical alkaline AAA battery [59], comfortably allowing fulfilment of Requirement F.4.

3.3.5: Data storage requirements

The device will store data on two different timescales: 1Hz and 8Hz. The air velocity reading will be taken eight times per second, with each measurement requiring 12 bits of storage. Adding this 96 bit-per-second load to the load imposed by the other sensors (106 bits, once per second) gives a total requirement of 202 bits-per-second. In a three-hour dive, this would generate approximately 0.27MB of data, which means that the device easily fulfils Requirement C.1 (c.f. Section 3.1.2).

Section 4: Processing for Variables of Interest

This section will outline how the raw data obtained from the sensors can be used to compute the three variables of interest in the smart regulator. Due to a shortage of time in the project, the device itself could not be robustly tested for its ability to carry out these operations. Nonetheless, this section aims to provide a sound theoretical framework by which experimental results could be processed to yield the variables of interest. In some cases, an open-source dataset [60], [61] was used to illustrate these principles though it should be noted that the conditions under which the data was obtained do not match the context in which a smart regulator would be used. Specifically, the data was obtained in a clinical setting from patients undergoing continuous positive airway pressure ventilation.

4.1 – Calculation of expired volume

The first of the three proposed functions is the calculation of expired air volume, allowing the diver to accurately track their gas depletion in real time. This will be accomplished by processing the output of the flow speed sensor (FS3000): as shown in Figure 9, the device will output a time-varying velocity signal indicating the air speed at the device inlet. The velocity is always positive because the use of umbrella valves at the device inlet prevent backflow during inspiration. Multiplying the air speed by the cross-sectional area of the channel yields the volume flow rate, expressed as a timeseries.

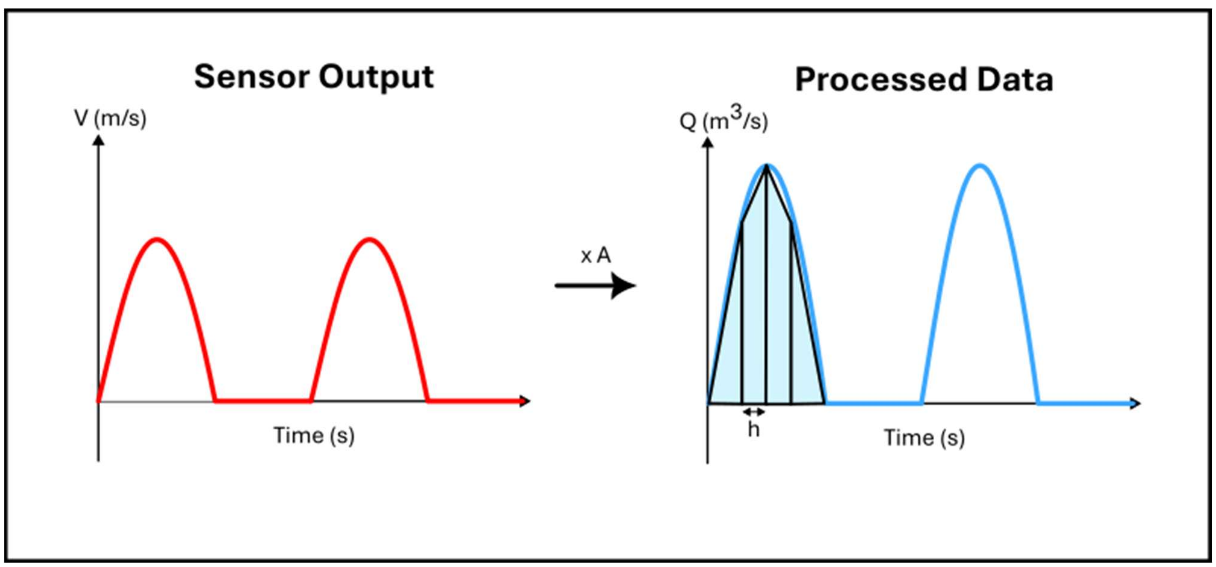

Figure 9: A schematic representation of the process for calculating expired volume using trapezoidal integration. This is the method that was employed to find the data used in Figure 10.

The final step in calculating the expired volume over a given time period is numerical integration using the trapezium rule, as illustrated in Figure 9. Though it is perhaps not as accurate as higher-order methods of numerical integration, it can be used to rapidly approximate the area under a curve whilst imposing a minimal computational load. Mathematically, the process to calculate expired volume (V) over time period T can be expressed as in Equation 2.

$$V = \int_0^T Q\,dt \approx \sum_{i=1}^{N-1} \frac{h}{2}(Q_i + Q_{i+1}) \qquad [2]$$

This method for finding expired volume was applied to the open-source dataset supplied by Guy *et al.* and appears to work reasonably well after some preprocessing of the data (see Appendix D for the code). Indeed, the mean volume exhaled in the first thirty seconds was 3.64 litres, which sits at the higher end of the normal physiological range [62]. However, this method also produced some results that are not consistent with normal respiration, as shown by the large spread of results in Figure 10. Since there is no way to objectively confirm the accuracy of the results, further testing is required to confirm the efficacy of the MATLAB algorithm.

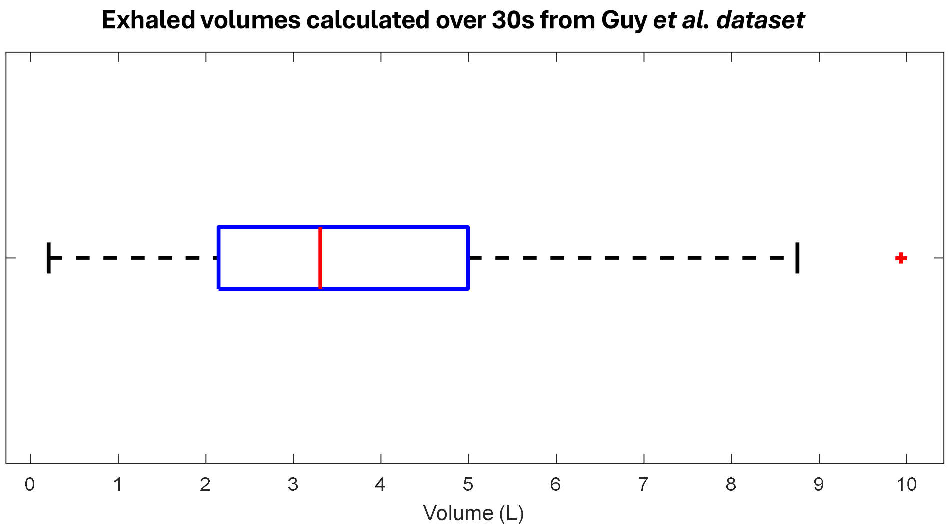

Figure 10: A boxplot showing the distribution of results obtained by applying the trapezium rule to the Guy et al. *open-source dataset.*

4.2 – Calculation of breathing rate

In theory, the development of an algorithm to find breathing rate should be simple: provided the flow sensor is operating properly, it should suffice to develop a program that counts the number of peaks (exhalations) in a given time period, then uses that number to compute the rate. However, as became clear during work with the Guy *et al.* dataset, respiratory data can be subject to significant noise, making it hard to determine the number of times an individual has exhaled.

Figure 11 provides a good illustration of this fact: whereas is easy to see that Figure 11a shows 7 exhalations, the number of exhalations is less readily apparent in Figure 11b. Indeed, the waveform in Figure 11b is so noisy that there is likely to be disagreement even amongst multiple human interpreters, potentially creating problems for validation.

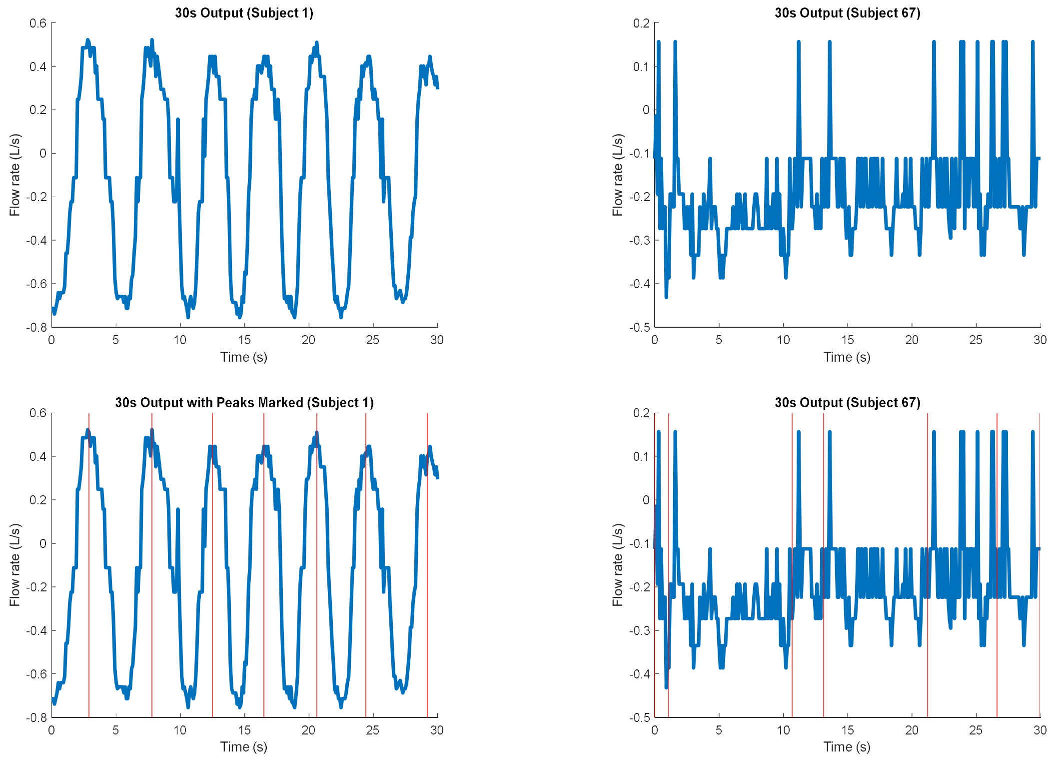

Figure 11a (top left), 11b (top right), 11c (bottom left), and 11d (bottom right): Figures 11a and b show thirty seconds of raw volume flow rate data from the Guy et al. *dataset. Figures 11c and 11d show the respiratory peaks, as defined by the algorithm (c.f. Appendix D for the code).*

Nonetheless, a simple algorithm was developed to count the number of breaths across the first thirty seconds of each recording. The MATLAB code for the program can be found in Appendix D. The program starts with a truncation step in which the top fifty percent of the rectified datapoints are isolated, followed by a smoothing operation that uses a moving average to remove noise. Finally, the maximum point of each of these peaks was used to define the peak of the exhalation: the mean time between these peaks provided the period of one cycle, allowing the breathing rate to be calculated.

Table 5: A tabulation of the difference between the human identified number of peaks and the algorithm-identified number of peaks across all eighty subjects.

Human identified breaths – algorithm identified breaths						
-4 or greater	-2 or -3	-1	0	+1	+2 or +3	+4 or greater
2	1	10	54	6	3	4

As shown in Table 5 above, the algorithm was able to identify the same number of peaks as the human analyst for most of the samples. However, there were several instances where there was quite extreme disagreement between the classifiers (four or more breaths in a thirty second sample). This fact alone does not indicate poor performance from either the human or the algorithm: as noted from the examination of Figure 11, there is no guarantee that the user-identified number of peaks is correct. The aim of this exercise was simply to explore one possible algorithm that could be used for peak breathing rate identification in the present study.

4.3 – Calculation of caloric expenditure

To calculate caloric expenditure, the proposed device intends to employ the modified Weir equation [13], [63] (c.f. Equation 3) which relates the rates of O_2 consumption ($V\dot{O}_2$) and CO_2 production ($VC\dot{O}_2$) to daily energy expenditure.

$$EE = 1.44 * (3.94 * V\dot{O}_2 + 1.1 * VC\dot{O}_2) \qquad [3]$$

Since these rates of production and consumption are expressed in terms of millilitres per minute, further processing is required to obtain their values from the concentration readings. Specifically, once concentration values for oxygen and carbon dioxide are obtained at time points t_1 ($[O_2]_1$ and $[CO_2]_1$) and t_2 ($[O_2]_2$ and $[CO_2]_2$), they must be averaged to find the mean concentrations over time period ΔT (where $\Delta T = t_2 - t_1$). These average concentrations ($[O_2]_{av}$ and $[CO_2]_{av}$) can be multiplied by the total expired volume V_e to obtain the total number of moles (nO_2 and nCO_2) expired in time period ΔT.

The volumes of gas expelled (VO_{2_1} and VCO_{2_1}) can then be calculated through use of the Ideal Gas Equation [64] (Equation 4). This requires the number of moles to be substituted in alongside the pressure (p), the universal gas constant (R), and the absolute temperature (T).

$$V_x = \frac{n_x RT}{p} \qquad [4]$$

The moles of O_2 consumed, and CO_2 produced, must be calculated by finding the difference between the inhaled volume and the exhaled volume, as in Equations 5 and 6. The inhaled volume would need to be estimated based on the exhaled volume, and the composition of the breathing gas.

$$\Delta VO_2 = O_2\ consumed\ = VO_{2_i} - VO_{2_1} \qquad [5]$$

$$\Delta V\mathrm{CO}_2 = CO_2\ produced\ = VCO_{2_1} - VCO_{2_i} \qquad [6]$$

Dividing these rates by the time period, as in Equations 7 and 8, provides the final values for $V\dot{O}_2$ and $VC\dot{O}_2$.

$$V\dot{O}_2 = \frac{\Delta VO_2}{\Delta T} \qquad [7]$$

$$VC\dot{O}_2 = \frac{\Delta VCO_2}{\Delta T} \qquad [8]$$

Caloric expenditure could not be directly tested from the open-source dataset since it lacked the required carbon dioxide and oxygen measurements. However, various forms of the modified Weir equation have served as the basis of energy expenditure calculation in several studies [13], [30], providing a strong basis on which to employ it in the present work.

Section 5: Discussion and Opportunities for Development

This section is split into three parts: the first will recapitulate and cross-examine the key findings of previous sections. Section 5.2 will then provide some information about the potential target market (recreational SCUBA divers) and will use this to discuss the commercial potential of the proposed device. Finally, Section 5.3 will list the main limitations of the present study.

5.1 – Discussion

Although this study originally aimed to design and test a full prototype of the device, the testing phase had to be omitted due to time constraints. Regardless, the present study provides significant value towards the broader aim of enhancing diver safety and wellbeing through breath analysis. Subsequent paragraphs will discuss the key findings of Sections 2, 3, and 4 to isolate important design lessons for breath analysis systems in SCUBA diving.

The literature review in Section 2 provided a strong scientific basis for the use of an indirect calorimetry and breath tracking device in the context of SCUBA diving, as well as some preliminary guidelines to direct subsequent design phases. Specifically, it was found that a mixing chamber approach to indirect calorimetry would likely allow energy expenditure to be calculated more accurately and affordably by removing the need for rapid sensor responses. In addition, the presence of flow-based breath tracking in some clinical studies provided compelling evidence that an air speed sensor could be employed to identify breathing rate in the smart regulator.

Section 3 built on the broad frameworks presented in Section 2 by laying out specific user and technical requirements for a SCUBA-based breath analysis device, then planning and validating a product to meet these demands. Designing the device required selection of commercially available components (sensors, battery, microcontroller, etc.) where possible, and creation of novel systems for housing the sensor array and isolating the required quantity of gas. Once devised, fulfilment of the technical requirements was assessed by means of mechanical and thermal simulations, as well as simpler numerical calculations to check the suitability of the power supply and data storage provisions. Overall, the findings suggest that a case made from 316L stainless steel and PET would provide the best performance for the lowest cost, though further field testing would be required to confirm this.

Finally, Section 4 explicitly connected the device outputs to achievement of the three stated device aims, thus providing a framework for achievement of the envisioned improvement in user safety and wellbeing. For two of these aims, Section 4 also used an open-source dataset to illustrate exactly how the sensor outputs could enable calculation of the relevant measurements. Although this work was fairly preliminary, it nonetheless showed significant potential for realisation of the aims outlined in Section 1.1. Thus, Section 4 provided the critical link between the stated objectives, and the theoretical work from Sections 2 and 3.

Based on these findings, it can be determined that the present work has made a meaningful contribution towards the development of a breath analysis device to enhance diver safety and wellbeing. Nonetheless, completion of this study represents the first step in a much longer process of product development and testing. Subsequent sections will describe the commercial potential of the device (Section 5.2), the shortcomings of the present work (Section 5.3), and potential opportunities for exploration and improvement (Section 6.2).

5.2 - Translational potential

This project has significant commercial potential due to its capacity to address an important unmet need in the diving industry. Specifically, by enhancing the safety and wellbeing of divers, the device has a unique and marketable value proposition which can be used to drive sales.

The SCUBA diving market is an attractive one in which to engage: the Professional Association of Diving Instructors (PADI) claims to certify more than one million divers each year [65], and it is estimated that the global dive tourism industry is worth about 36 billion USD annually [66]. Furthermore, people who partake in SCUBA diving typically have a high income compared to non-divers [67], and figures from one industry body suggest that recreational divers spend more than 300 USD on diving gear annually [68] (technical divers spend far more).

*Table 6: A breakdown of the raw material costs for a single unit. Note that the cost of the PCB has been omitted. Entries marked with a * denote values converted from USD using a rate of 1 GBP = 0.76 USD.*

Item	Qty.	Unit cost (GBP)	Total cost (GBP)
316L Stainless Steel (kg)	2.28	3.02	6.89*
PET (kg)	0.14	0.55	0.08*
Bosch BME680	1	10.33	10.33
Renesas FS3000	1	19.67	19.67
SGX-4OX-ROHS	1	58.99	58.99
Sensirion STC31	1	50.98	50.98
Adafruit ESP32-S3 TFT Feather	1	15.16*	15.16*
Total (GBP):			162.10

Table 6 shows the material costs associated with the production of a single unit, giving a total price of 162.10 GBP. Naturally, this figure will be refined with the incorporation of labour and processing costs, as well as discounts enabled by bulk ordering of sensors and raw materials. Nonetheless, this first estimate suggests that unit cost will be appropriate to the target market, even including a 50% or 100% markup to drive profit. Now that this study has established a theoretical basis for the smart regulator, further research should be conducted to verify that demand exists amongst members of the target market.

5.3 – Limitations of the present study

Despite the achievements of this study, there are several limitations in the methodology that should be considered when undertaking subsequent work. Chief among these is the absence of testing to show that the specific components and systems described in Section 3 provide the data required to accurately complete the calculations detailed in Section 4. As Section 6.2 will outline, addressing this shortcoming should be the first priority of subsequent work on this project since this will provide an essential starting point for any further refinement of the design.

A second weakness of this study is the use of open-source data that was collected from patients undergoing positive-pressure ventilation, a context markedly different to the environment in which the device is intended to operate. As such, even though Section 4 provides a useful theoretical starting point for analysis of relevant respiratory data, the flow signals obtained from SCUBA divers are likely to have very different characteristics.

A third and final limitation of the method used in this study lies in the fact that no verification step was included to assess whether the outputs of the algorithms employed in Section 4 reflected the true state of events (i.e. the volume of expired air or exhalations in thirty seconds). Although the lack of an appropriate dataset meant that this could not be avoided, the use of an alternative testing method could have provided a means to more objectively assess the performance of the selected algorithms.

Section 6: Conclusion and Suggestions for Further Work

6.1 – Conclusion

To conclude, this work provides a compelling justification for the implementation of a breath analysis system in the context of SCUBA diving, as well as a detailed framework for the realisation of such a device. The report began with a description of the main challenges to safety and wellbeing, followed by an outline of the key technical characteristics required by an appropriate solution. A review in Section 2 then provided some preliminary design guidelines through an examination of existing literature in the areas of indirect calorimetry and respiratory rate monitoring. The start of Section 3 expanded these guidelines into a detailed set of user and technical requirements, concretising the necessary device characteristics. The remainder of Section 3 proposed and tested a solution that could address all these demands, using numerical calculations and simulations as a means of validation. Section 4 then linked the envisioned device outputs to the parameters of interest, confirming that the proposed device should enable achievement of its three intended aims. Finally, Section 5 discussed the main findings and limitations of the present study, alongside a brief overview of the commercial potential of the smart regulator.

6.2 – Suggestions for further work

As alluded to in Section 5.3, further work on this project should first focus on testing and refining the present prototype. This will ensure that the device is capable of fulfilling the three desired functions and is ready to move towards further optimisation for field testing, mass production, and commercialisation. Given the high-risk environment which the product is intended for, it is essential that the testing phases be iterative and gradual, with each successive stage more closely approximating the true context of SCUBA diving. A reasonable first step would be to test the prototype using dry, compressed gases in a laboratory setting. This could be followed by work using humidified gases, then human exhaled breath in order to assess the suitability of the sensors for this application. The environmental conditions should also be gradually altered to match the target context, enabling an assessment of factors like waterproofing and pressure tolerance. Ideally, this should be done using shallow water or a hyperbaric chamber to remedy any safety issues before moving to field testing.

Ultimately, it is hoped that a smart regulator will become an indispensable safety tool for recreational divers. However, to achieve this aim, it is essential that the device be made as convenient and user-friendly as possible. One way to do this would be to entirely integrate the sensor array and mixing chamber into the existing structure of a second-stage regulator. An example of how this could be realised is shown in Figure 12: as can be seen, the body of the regulator is split into two parts separated by an umbrella valve. As the diver exhales, most of the air leaves the regulator via the main exhaust, but a small sample is passed to the sensor array in the front of the regulator by a second umbrella valve. Although this vision is somewhat removed from the results of the present study, it is important to remember that commercial success is predicated on accounting for the needs of the target market. Thus, usability considerations such as this will be central to maximising sales and, ultimately, the benefit to diver safety and wellbeing achieved through use of the product.

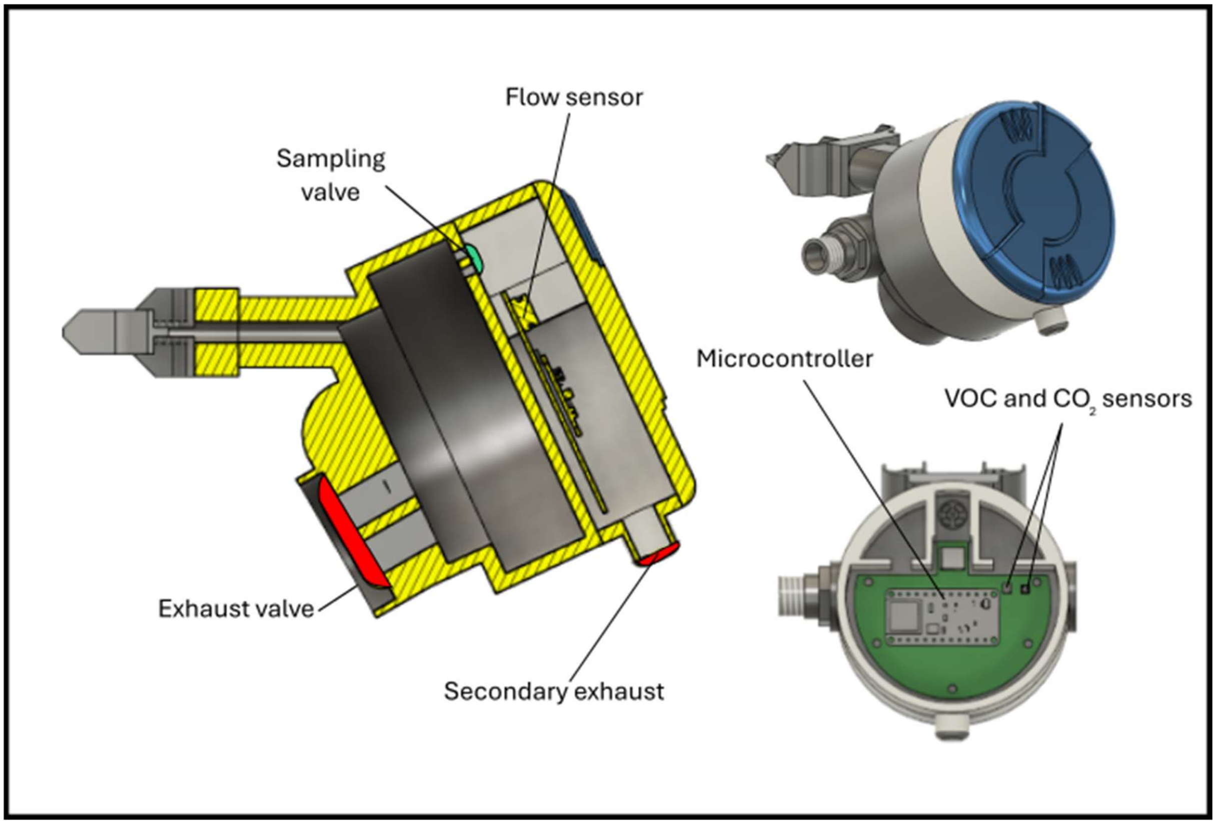

Figure 12: A Fusion-360 model of a potential improvement on the present design. In this case, the sensor array is housed entirely in the second-stage regulator.

References

[1] T. Santiago Perez, B. M. Crowe, P. J. Rosopa, J. N. Townsend, and M. R. Kaufman, 'Diving into Health: A Mixed Methods Study on the Impact of Scuba Diving in People with Physical Impairments', *Healthcare*, vol. 11, no. 7, p. 984, Mar. 2023, doi: 10.3390/healthcare11070984.

[2] A. Carreño, M. Gascon, C. Vert, and J. Lloret, 'The Beneficial Effects of Short-Term Exposure to Scuba Diving on Human Mental Health', *Int. J. Environ. Res. Public. Health*, vol. 17, no. 19, p. 7238, Oct. 2020, doi: 10.3390/ijerph17197238.

[3] D. Penrice and J. S. Cooper, 'Diving Casualties', in *StatPearls*, Treasure Island (FL): StatPearls Publishing, 2023.

[4] N. Smith, 'Scuba Diving: How High the Risk?', *J. Insur. Med.*, vol. 27, no. 1, 1995.

[5] B. Bube, B. B. Zanón, A. M. Lara Palma, and H. Klocke, 'Wearable Devices in Diving: Scoping Review', *JMIR MHealth UHealth*, vol. 10, no. 9, p. e35727, Sep. 2022, doi: 10.2196/35727.

[6] S. Lucrezi *et al.*, 'Safety Priorities and Underestimations in Recreational Scuba Diving Operations: A European Study Supporting the Implementation of New Risk Management Programmes', *Front. Psychol.*, vol. 9, p. 383, Mar. 2018, doi: 10.3389/fpsyg.2018.00383.

[7] P. Buzzacott, Ed., *DAN Annual Diving Report 2017 Edition: A Report on 2015 Diving Fatalities, Injuries, and Incidents*. in Divers Alert Network Annual Diving Reports. Durham (NC): Divers Alert Network, 2017. Accessed: Jun. 19, 2024. [Online]. Available: http://www.ncbi.nlm.nih.gov/books/NBK487739/

[8] P. J. Denoble, Ed., *DAN Annual Diving Report 2019 Edition: A report on 2017 diving fatalities, injuries, and incidents*. in Divers Alert Network Annual Diving Reports. Durham (NC): Divers Alert Network, 2019. Accessed: Jun. 19, 2024. [Online]. Available: http://www.ncbi.nlm.nih.gov/books/NBK562527/

[9] C. J. Edge and P. T. Wilmshurst, 'The pathophysiologies of diving diseases', *BJA Educ.*, vol. 21, no. 9, pp. 343–348, Sep. 2021, doi: 10.1016/j.bjae.2021.05.003.

[10] C. Altepe, S. Egi, T. Ozyigit, D. Sinoplu, A. Marroni, and P. Pierleoni, 'Design and Validation of a Breathing Detection System for Scuba Divers', *Sensors*, vol. 17, no. 6, p. 1349, Jun. 2017, doi: 10.3390/s17061349.

[11] J. Gardner and T. Vincent, 'Electronic Noses for Well-Being: Breath Analysis and Energy Expenditure', *Sensors*, vol. 16, no. 7, p. 947, Jun. 2016, doi: 10.3390/s16070947.

[12] P. Mochalski *et al.*, 'Non-contact breath sampling for sensor-based breath analysis', *J. Breath Res.*, vol. 13, no. 3, p. 036001, Apr. 2019, doi: 10.1088/1752-7163/ab0b8d.

[13] H. P. F. X. Moonen, K. J. H. Beckers, and A. R. H. Van Zanten, 'Energy expenditure and indirect calorimetry in critical illness and convalescence: current evidence and practical considerations', *J. Intensive Care*, vol. 9, no. 1, p. 8, Jan. 2021, doi: 10.1186/s40560-021-00524-0.

[14] J. D. Pleil, M. Ariel Geer Wallace, M. D. Davis, and C. M. Matty, 'The physics of human breathing: flow, timing, volume, and pressure parameters for normal, on-demand, and ventilator respiration', *J. Breath Res.*, vol. 15, no. 4, p. 042002, Oct. 2021, doi: 10.1088/1752-7163/ac2589.

[15] S. Das and M. Pal, 'Review—Non-Invasive Monitoring of Human Health by Exhaled Breath Analysis: A Comprehensive Review', *J. Electrochem. Soc.*, vol. 167, no. 3, p. 037562, Jan. 2020, doi: 10.1149/1945-7111/ab67a6.

[16] M. R. Mhetre and H. K. Abhyankar, 'Human exhaled air energy harvesting with specific reference to PVDF film', *Eng. Sci. Technol. Int. J.*, vol. 20, no. 1, pp. 332–339, Feb. 2017, doi: 10.1016/j.jestch.2016.06.012.

[17] E. Mansour *et al.*, 'Measurement of temperature and relative humidity in exhaled breath', *Sens. Actuators B Chem.*, vol. 304, p. 127371, Feb. 2020, doi: 10.1016/j.snb.2019.127371.

[18] R. C. Roche *et al.*, 'Recreational Diving Impacts on Coral Reefs and the Adoption of Environmentally Responsible Practices within the SCUBA Diving Industry', *Environ. Manage.*, vol. 58, no. 1, pp. 107–116, Jul. 2016, doi: 10.1007/s00267-016-0696-0.

[19] S. Priem, J. Jonckheer, E. De Waele, and J. Stiens, 'Indirect Calorimetry in Spontaneously Breathing, Mechanically Ventilated and Extracorporeally Oxygenated Patients: An Engineering Review', *Sensors*, vol. 23, no. 8, p. 4143, Apr. 2023, doi: 10.3390/s23084143.

[20] D. J. Macfarlane, 'Open-circuit respirometry: a historical review of portable gas analysis systems', *Eur. J. Appl. Physiol.*, vol. 117, no. 12, pp. 2369–2386, Dec. 2017, doi: 10.1007/s00421-017-3716-8.

[21] L. M. Candell *et al.*, 'Low Cost Metabolic Fuel Sensor for On-Demand Personal Health and Fitness Tracking', Bioengineering, preprint, Feb. 2020. doi: 10.1101/2020.02.20.958264.

[22] H. C. Pinnington, P. Wong, J. Tay, D. Green, and B. Dawson, 'The Level of Accuracy and Agreement in Measures of FsO2, FBCO2and Vs Between the Cosmed K4b2 Portable, Respiratory Gas Analysis System and a Metabolic Cart', 2001.

[23] R. Duffield, B. Dawson, H. Pinnington, and P. Wong, ‘Accuracy and reliabillity of a Cosmed K4b2 portable gas analysis system’.

[24] A. J. Vogler, A. J. Rice, and C. J. Gore, ‘Validity and reliability of the Cortex MetaMax3B portable metabolic system’, *J. Sports Sci.*, vol. 28, no. 7, pp. 733–742, May 2010, doi: 10.1080/02640410903582776.

[25] D. J. Macfarlane and P. Wong, ‘Validity, reliability and stability of the portable Cortex Metamax 3B gas analysis system’, *Eur. J. Appl. Physiol.*, vol. 112, no. 7, pp. 2539–2547, Jul. 2012, doi: 10.1007/s00421-011-2230-7.

[26] I. Perez-Suarez *et al.*, ‘Accuracy and Precision of the COSMED K5 Portable Analyser’, *Front. Physiol.*, vol. 9, p. 1764, Dec. 2018, doi: 10.3389/fphys.2018.01764.

[27] S. E. Crouter, S. R. LaMunion, P. R. Hibbing, A. S. Kaplan, and D. R. Bassett, ‘Accuracy of the Cosmed K5 portable calorimeter’, *PLOS ONE*, vol. 14, no. 12, p. e0226290, Dec. 2019, doi: 10.1371/journal.pone.0226290.

[28] C. Beijst, G. Schep, E. V. Breda, P. F. F. Wijn, and C. V. Pul, ‘Accuracy and precision of CPET equipment: A comparison of breath-by-breath and mixing chamber systems’, *J. Med. Eng. Technol.*, vol. 37, no. 1, pp. 35–42, Jan. 2013, doi: 10.3109/03091902.2012.733057.

[29] K. Winkert, J. Kirsten, J. Dreyhaupt, J. M. Steinacker, and G. Treff, ‘The COSMED K5 in Breath-by-Breath and Mixing Chamber Mode at Low to High Intensities’, *Med. Sci. Sports Exerc.*, vol. 52, no. 5, pp. 1153–1162, May 2020, doi: 10.1249/MSS.0000000000002241.

[30] T. A. Vincent, A. Wilson, J. G. Hattersley, M. J. Chappell, and J. W. Gardner, ‘Development of a Handheld Side-Stream Breath Analyser for Point of Care Metabolic Rate Measurement’, in *Bioinformatics and Biomedical Engineering*, vol. 9656, F. Ortuño and I. Rojas, Eds., in Lecture Notes in Computer Science, vol. 9656. , Cham: Springer International Publishing, 2016, pp. 13–21. doi: 10.1007/978-3-319-31744-1_2.

[31] S. J. Eun, J. Y. Kim, and S. H. Lee, ‘Development of Customized Diving Computer Based on Wearable Sensor for Marine Safety’, *IEEE Access*, vol. 7, pp. 17951–17957, 2019, doi: 10.1109/ACCESS.2019.2894740.

[32] A. Nicolò, C. Massaroni, E. Schena, and M. Sacchetti, ‘The Importance of Respiratory Rate Monitoring: From Healthcare to Sport and Exercise’, *Sensors*, vol. 20, no. 21, p. 6396, Nov. 2020, doi: 10.3390/s20216396.

[33] A. Nicolò, C. Massaroni, and L. Passfield, ‘Respiratory Frequency during Exercise: The Neglected Physiological Measure’, *Front. Physiol.*, vol. 8, p. 922, Dec. 2017, doi: 10.3389/fphys.2017.00922.

[34] D. Vitazkova *et al.*, ‘Advances in Respiratory Monitoring: A Comprehensive Review of Wearable and Remote Technologies’, *Biosensors*, vol. 14, no. 2, p. 90, Feb. 2024, doi: 10.3390/bios14020090.

[35] C. Massaroni, A. Nicolò, D. Lo Presti, M. Sacchetti, S. Silvestri, and E. Schena, ‘Contact-Based Methods for Measuring Respiratory Rate’, *Sensors*, vol. 19, no. 4, p. 908, Feb. 2019, doi: 10.3390/s19040908.

[36] T. Jiang *et al.*, ‘Wearable Airflow Sensor for Nasal Symmetric Evaluation and Respiration Monitoring’, in *2019 IEEE SENSORS*, Montreal, QC, Canada: IEEE, Oct. 2019, pp. 1–4. doi: 10.1109/SENSORS43011.2019.8956504.

[37] T. Lin, X. Lv, Z. Hu, A. Xu, and C. Feng, ‘Semiconductor Metal Oxides as Chemoresistive Sensors for Detecting Volatile Organic Compounds’, *Sensors*, vol. 19, no. 2, p. 233, Jan. 2019, doi: 10.3390/s19020233.

[38] P. T. Moseley, ‘Progress in the development of semiconducting metal oxide gas sensors: a review’, *Meas. Sci. Technol.*, vol. 28, no. 8, p. 082001, Aug. 2017, doi: 10.1088/1361-6501/aa7443.

[39] G. Wypych, *Handbook of polymers*. Toronto: ChemTec Pub, 2012.

[40] A. R. Bagheri, C. Laforsch, A. Greiner, and S. Agarwal, ‘Fate of So-Called Biodegradable Polymers in Seawater and Freshwater’, *Glob. Chall.*, vol. 1, no. 4, p. 1700048, Jul. 2017, doi: 10.1002/gch2.201700048.

[41] H. Tian, F. Wu, P. Chen, X. Peng, and H. Fang, ‘Microwave-assisted *in situ* polymerization of polycaprolactone/boron nitride composites with enhanced thermal conductivity and mechanical properties’, *Polym. Int.*, vol. 69, no. 7, pp. 635–643, Jul. 2020, doi: 10.1002/pi.6000.

[42] N. Atanasova *et al.*, ‘Degradation of Poly(ε-caprolactone) by a Thermophilic Community and Brevibacillus thermoruber Strain 7 Isolated from Bulgarian Hot Spring’, *Biomolecules*, vol. 11, no. 10, p. 1488, Oct. 2021, doi: 10.3390/biom11101488.

[43] G. Spinelli, R. Kotsilkova, E. Ivanov, V. Georgiev, C. Naddeo, and V. Romano, ‘Thermal and Dielectric Properties of 3D Printed Parts Based on Polylactic Acid Filled with Carbon Nanostructures’, *Macromol. Symp.*, vol. 405, no. 1, p. 2100244, Oct. 2022, doi: 10.1002/masy.202100244.

[44] C. Wellenreuther, A. Wolf, and N. Zander, ‘Cost competitiveness of sustainable bioplastic feedstocks – A Monte Carlo analysis for polylactic acid’, *Clean. Eng. Technol.*, vol. 6, p. 100411, Feb. 2022, doi: 10.1016/j.clet.2022.100411.

[45] A. Singh *et al.*, ‘Techno-economic, life-cycle, and socioeconomic impact analysis of enzymatic recycling of poly(ethylene terephthalate)’, *Joule*, vol. 5, no. 9, pp. 2479–2503, Sep. 2021, doi: 10.1016/j.joule.2021.06.015.

[46] P. D. Harvey and American Society for Metals, Eds., *Engineering properties of steel*. Metals Park, Ohio: American Society for Metals, 1982.

[47] J. Chen, Q. Zhang, Q. Li, S. Fu, and J. Wang, ‘Corrosion and tribocorrosion behaviors of AISI 316 stainless steel and Ti6Al4V alloys in artificial seawater’, *Trans. Nonferrous Met. Soc. China*, vol. 24, no. 4, pp. 1022–1031, Apr. 2014, doi: 10.1016/S1003-6326(14)63157-5.

[48] S. Gupta, D. Singh, A. Yadav, S. Jain, and B. Pratap, ‘A comparative study of 5083 aluminium alloy and 316L stainless steel for shipbuilding material’, *Mater. Today Proc.*, vol. 28, pp. 2358–2363, 2020, doi: 10.1016/j.matpr.2020.04.641.

[49] A. A. Adediran, A. A. Akinwande, O. A. Balogun, O. S. Adesina, A. Olayanju, and T. Mojisola, ‘Evaluation of the properties of Al-6061 alloy reinforced with particulate waste glass’, *Sci. Afr.*, vol. 12, p. e00812, Jul. 2021, doi: 10.1016/j.sciaf.2021.e00812.

[50] N. Santhosh *et al.*, ‘Analysis of friction and wear of aluminium AA 5083/ WC composites for building applications using advanced machine learning models’, *Ain Shams Eng. J.*, vol. 14, no. 9, p. 102090, Sep. 2023, doi: 10.1016/j.asej.2022.102090.

[51] H. Ezuber, A. El-Houd, and F. El-Shawesh, ‘A study on the corrosion behavior of aluminum alloys in seawater’, *Mater. Des.*, vol. 29, no. 4, pp. 801–805, Jan. 2008, doi: 10.1016/j.matdes.2007.01.021.

[52] J. R. Davis and ASM International, Eds., *Aluminum and aluminum alloys*, 6. print. in ASM specialty handbook. Materials Park, Ohio: ASM International, 2007.

[53] S. Pal *et al.*, ‘Evolution of the metallurgical properties of Ti-6Al-4V, produced with different laser processing parameters, at constant energy density in selective laser melting’, *Results Phys.*, vol. 17, p. 103186, Jun. 2020, doi: 10.1016/j.rinp.2020.103186.

[54] B. Baufeld and O. Van Der Biest, ‘Mechanical properties of Ti-6Al-4V specimens produced by shaped metal deposition’, *Sci. Technol. Adv. Mater.*, vol. 10, no. 1, p. 015008, Jan. 2009, doi: 10.1088/1468-6996/10/1/015008.

[55] L. Bolzoni, E. M. Ruiz-Navas, and E. Gordo, ‘Flexural properties, thermal conductivity and electrical resistivity of prealloyed and master alloy addition powder metallurgy Ti–6Al–4V’, *Mater. Des. 1980-2015*, vol. 52, pp. 888–895, Dec. 2013, doi: 10.1016/j.matdes.2013.06.036.

[56] G. Senopati, R. A. Rahman Rashid, I. Kartika, and S. Palanisamy, ‘Recent Development of Low-Cost β-Ti Alloys for Biomedical Applications: A Review’, *Metals*, vol. 13, no. 2, p. 194, Jan. 2023, doi: 10.3390/met13020194.

[57] S. Hallett, F. Toro, and J. V. Ashurst, ‘Physiology, Tidal Volume’, in *StatPearls*, Treasure Island (FL): StatPearls Publishing, 2024.

[58] V. Gladkikh and R. Tenzer, ‘A Mathematical Model of the Global Ocean Saltwater Density Distribution’, *Pure Appl. Geophys.*, vol. 169, no. 1–2, pp. 249–257, Jan. 2012, doi: 10.1007/s00024-011-0275-5.

[59] K. Mikhaylov, J. Tervonen, and D. Fadeev, ‘Development of Energy Efficiency Aware Applications Using Commercial Low Power Embedded Systems’, in *Embedded Systems - Theory and Design Methodology*, K. Tanaka, Ed., InTech, 2012. doi: 10.5772/38171.

[60] E. F. S. Guy *et al.*, ‘Respiratory dataset from PEEP study with expiratory occlusion’. PhysioNet. doi: 10.13026/D767-E709.

[61] A. L. Goldberger *et al.*, ‘PhysioBank, PhysioToolkit, and PhysioNet: Components of a New Research Resource for Complex Physiologic Signals’, *Circulation*, vol. 101, no. 23, Jun. 2000, doi: 10.1161/01.CIR.101.23.e215.

[62] *Principles of Pulmonary Medicine*. Elsevier, 2014. doi: 10.1016/C2010-0-69638-6.

[63] J. B. D. V. Weir, ‘New methods for calculating metabolic rate with special reference to protein metabolism’, *J. Physiol.*, vol. 109, no. 1–2, pp. 1–9, Aug. 1949, doi: 10.1113/jphysiol.1949.sp004363.

[64] K. M. Tenny and J. S. Cooper, ‘Ideal Gas Behavior’, in *StatPearls*, Treasure Island (FL): StatPearls Publishing, 2024.

[65] The Professional Association of Diving Instructors (PADI), ‘About PADI’, PADI. Accessed: Aug. 22, 2024. [Online]. Available: https://www.padi.com/about-padi

[66] Z. A. Nisa, C. Schofield, and F. C. Neat, ‘Work Below Water: The role of scuba industry in realising sustainable development goals in small island developing states’, *Mar. Policy*, vol. 136, p. 104918, Feb. 2022, doi: 10.1016/j.marpol.2021.104918.

[67] S. I. Ranapurwala, K. L. Kucera, and P. J. Denoble, ‘The healthy diver: A cross-sectional survey to evaluate the health status of recreational scuba diver members of Divers Alert Network (DAN)’, *PLOS ONE*, vol. 13, no. 3, p. e0194380, Mar. 2018, doi: 10.1371/journal.pone.0194380.

[68] Business of Diving Institute, ‘Survey Results: How Much Scuba Divers Spend Annually on Dive Gear, Travel, Training & Services - Business of Diving Institute’. Accessed: Aug. 22, 2024. [Online]. Available: https://www.businessofdiving.com/how-much-scuba-divers-spend-annually-dive-gear-travel-courses

[69] B. Pattanayak, S. S. Lal, and H. B. Kothadia, ‘Natural convection heat transfer from upward-facing plates in saline water’, *Heat Transf.*, vol. 52, no. 6, pp. 3896–3913, Sep. 2023, doi: 10.1002/htj.22857.

Appendix A: Sensor Properties

Table 7: A tabulation of relevant sensor properties.

Sensor name	Variable	Type	Estimated power (mW)	Range	Price (GBP)
STC31	$[CO_2]$	Thermal conductivity	9.9	0-100%	50.98
	Temperature			-20 - +85°C	
SGX-4OX-ROHS	$[O_2]$	Electrochemical	6.0	0-25%	58.99
BME680	Pressure	Metal oxide	21.6	0.3 – 1.1 bar	10.33
	Humidity			0-100% r.H.	
	Temperature			-40 - +85°C	
	$[VOC]$			>5ppm	
Renesas FS3000	Air velocity	Air velocity	33	0 – 15 ms^{-1}	19.67
				Total:	139.97

Table 8: A tabulation of relevant sensor properties.

Sensor name	Variable	Response Time	Resolution (bit)	Frequency (Hz)	Interface
STC31	$[CO_2]$	$T_{63} < 2s$	16	1	I^2C
	Temperature		16		
SGX-4OX-ROHS	$[O_2]$	$T_{90} < 10s$*	10	1	ADC1/DAC1
BME680	Pressure	Not given	20	1	I^2C
	Humidity	$T_{63} < 8s$	16		
	Temperature	Not given	20		
	$[VOC]$	$T_{33\text{-}36} < 1s$	8		
Renesas FS3000	Temperature	125 ms	12	8	I^2C

Appendix B: Details of Thermal Simulations

The thermal simulations in this study were intended to simulate the effects of applying a thermal shock to the case: this was done using a transient thermal analysis on Abaqus. To make the modelling simpler, the case lid was excluded from the simulations. At the beginning of each test, the case was modelled as being in thermal equilibrium with hot surroundings (35 degrees Celsius). During the simulation phase, a thermal shock was applied to the system in the form of a convective heat loss from the outer surfaces. The sink temperature was set to 5, 15, and 25 degrees Celsius to model different sizes of thermal shock. In all cases, the film coefficient was estimated as 2000 W/(m^2K) based on the findings of a 2023 study by Pattanayak, Lal, and Kothadia [69]: although the film coefficient for convective heat transfer from a plastic surface is likely to be different, no reliable figure could be found. A “tie” constraint was applied between the inner surfaces of the shell and the outer surfaces of the inner frame as shown in Figure 13, thus allowing heat transfer to occur between the bodies.

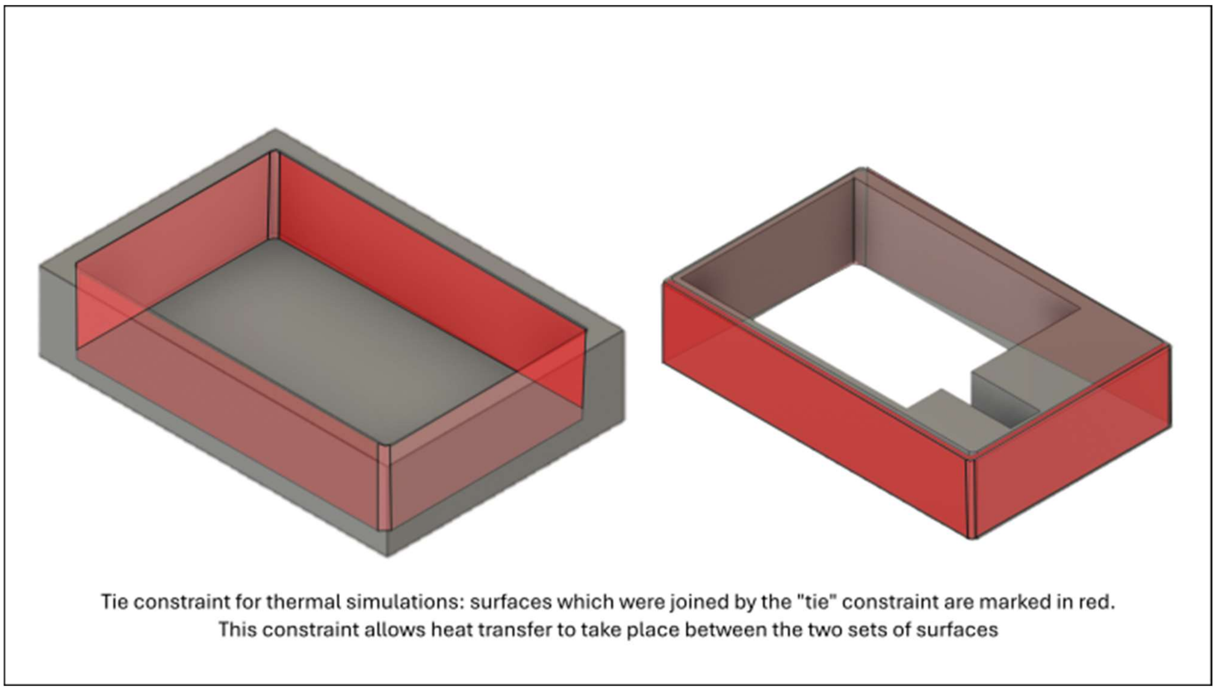

Figure 13: An illustration showing where the "tie" constraint was applied during the thermal shock simulations.

Table 9: A tabulation of relevant simulation parameters for the thermal shock studies.

Parameter	Specification
Number of elements	13169
Element shape	Tetrahedral
Space function order	Quadratic
Adaptive mesh refinement	None
Simulation time period	1000 seconds
Incrementation	20 seconds

Appendix C: Details of Mechanical Simulations

Since the total force exerted by hydrostatic pressure is dependent on the area of the surface, each of the relevant surface areas had to be calculated to obtain the compressive load. The single-letter designations of each surface are shown in Figure 14. Note that, although surface X is structurally similar to B, it was designated as the fixed support and thus had no load applied to it. The compressive load applied to each surface at the two test depths is provided in Table 10. Further details required for simulation are provided in Table 11: these parameters were chosen with the aim of robustly simulating the required scenarios without exceeding the computational capacities of the Author's personal computer.

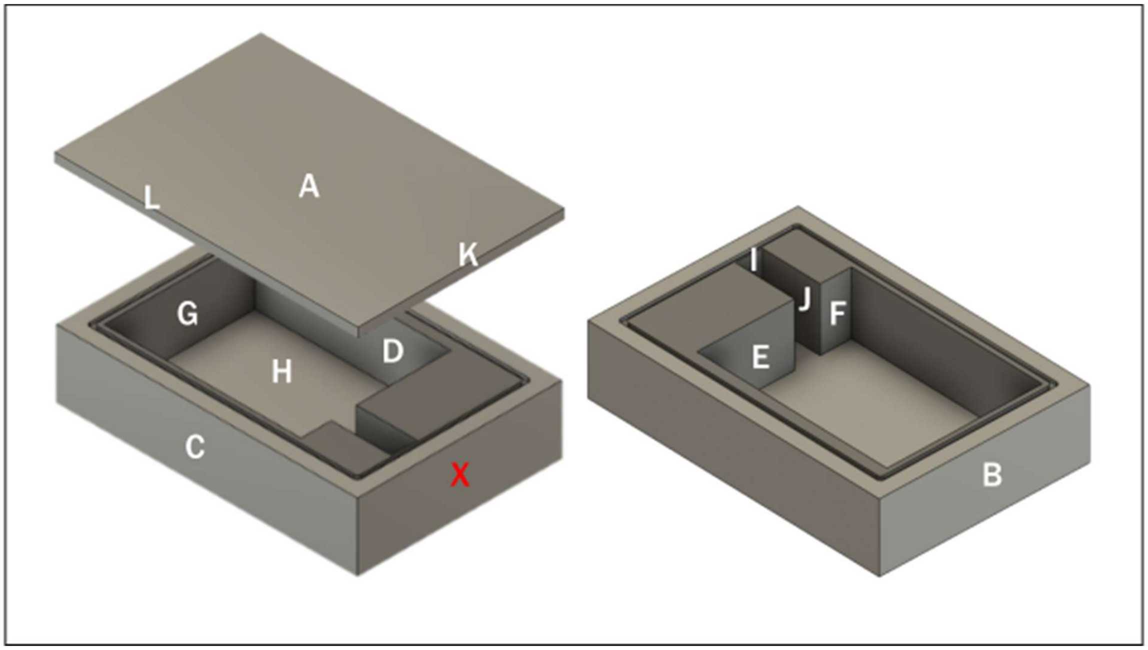

Figure 14: A diagram showing the letter designations of the surfaces in the device: surfaces that have the same dimensions share the same designation. Note that the interior of the device has been recoloured to make the diagram easier to understand.

Table 10: A tabulation of the forces applied to the surfaces of the device, as labelled in Figure 14.

Surface	Count	Dimension 1 (mm)	Dimension 2 (mm)	Force at 30m (N)	Force at 60m (N)
A	3	163.55	111.05	5345	10690
B	1	111.05	36.75	1201	2402
C	2	163.55	36.75	1769	3538
D	2	106.50	33.75	1058	2116
E	1	51.50	33.75	512	1023
F	1	16.50	33.75	164	328
G	1	82.00	33.75	814	1629
H	1	95.05	147.55	4127	8255
I	1	14.00	33.75	139	278
J	2	32.50	33.75	323	646
K	2	5.00	111.05	163	327
L	2	5.00	163.55	241	481

Table 11: A tabulation of relevant simulation parameters used in the static stress studies.

Parameter	Specification
Number of elements	69155
Element shape	Tetrahedral
Space function order	Parabolic
Automatic contact detection tolerance	0.05mm
Minimum element size as a percentage of average size	20
Adaptive mesh refinement	None

Appendix D: Code from Section 4

```
%% ===== Full Dataset Breath Number Finder ================================

% ===== Load all 80 breathing datasets ====================================
for j = 1:80
    clearvars -except auc_all_subj alg_30s_breaths alg_br_rate j


    leaf = num2str(j);
    stem = 'ProcessedData_Subject';
    extension = '.csv';
    filename = strcat(stem,leaf,extension);

    sprintf('Subject Number %i', j)

    % ====== Import data ==================================================
    table = readtable(filename);
    data = table2array(readtable(filename));

    round_time = (round(data(:,1),1));

    % ====== Isolate one datapoint per time 0.1s ==========================
    mark = 0;
    count = 1;
    for i = 1:length(data(:,1))

        if round(round_time(i),1) == round(mark,1)
            graph_time(count) = round_time(i);
            trunc_flow(count) = -data(i,3);
            mark = mark + 0.1;
            count = count + 1;
        end


    end


    % ====== Find number of breaths in first 30s ==========================
    breath_30s = trunc_flow(1:301);

    breath_30s_rect = max(breath_30s,0); % set all negative entries to zero

    breath_30s_peaks = max(breath_30s,0); % set all negative entries to zero
    breath_30s_peaks(breath_30s_peaks < 0.50*max(breath_30s_peaks)) = 0; % set all
values less than 50% of max to zero
    breath_30s_peaks = movmean(breath_30s_peaks,11);

    % ===== Isolate all waveforms =========================================
    count = 1;
    row = 1;
    col = 1;
    for i = 1:length(breath_30s_peaks) - 1

        if breath_30s_peaks(i) ~= 0
            waves(row,col) = breath_30s_peaks(i);
            locs(row,col) = i;
            row = row + 1;
        end

        if breath_30s_peaks(i + 1) == 0 && breath_30s_peaks(i) ~= 0
```

```
            row = 1;
            col = col + 1;
        end
    end

    % ===== Find max of each waveform ====================================
    [peaklength peaknum] = size(waves);

    waves(:,all(waves == 0)) = [];
    [peaklength peaknum] = size(waves);
    for i = 1:peaknum
        w_temp = waves(:,i);
        [wmax_val wmax_pt] = max(w_temp);
        full_locs(i) = locs(wmax_pt,i);
    end

    time_30s = 0:0.1:30;
    full_times = time_30s(full_locs);


    % ===== Calculate breathing rate ======================================
    peak_dist = diff(full_locs);
    avg_dist = mean(peak_dist);
    breath_interval = avg_dist/10;
    br_rate = 60/breath_interval;
    round_br_rate = round(br_rate);


    % ===== Calculate area under the curve (AUC) ==========================
    breath_30s_rect = movmean(breath_30s_rect,11);
    for i = 1:length(breath_30s_rect) - 1
        a_slice(i) = 0.05*(breath_30s_rect(i)+breath_30s_rect(i+1));
    end
    auc = sum(a_slice);

    % ===== Create full datasets ==========================================
    auc_all_subj(j) = auc;
    alg_30s_breaths(j) = peaknum;
    alg_br_rate(j) = br_rate;

end

clearvars -except auc_all_subj alg_30s_breaths alg_br_rate j

% ===== Import user guesses ==============================================
load('user_br_num_30s_exhales.mat')
user_breaths = str2double(user_br_num_30s);

% ===== Calculate error between human and algorithm ======================
delt = user_breaths - alg_30s_breaths;
num_perfect = nnz(~delt);

% ===== Calculate the spread of errors ===================================
unique_errors = unique(delt);
freq_errors = [unique_errors' histc(delt(:),unique_errors)];
```